Sciences of Geodesy - II

Innovations and Future Developments

Bearbeitet von
Guochang Xu

schnell und portofrei erhältlich bei

beck-shop.de
DIE FACHBUCHHANDLUNG

Chapter 2
General Relativity and Space Geodesy

Ludwig Combrinck

1 Background

Newton's final version (published in 1726) of *Philosophiae Naturalis Principia Mathematica* was a great scientific achievement of the time and contained sufficient information to allow calculation of the dynamics of terrestrial and celestial bodies; it also expounded on the absolute nature of time and space. As examples, Newton's statements (Newton 1726) that *"Absolute, true, and mathematical time, of itself, and from its own nature flows equably without regard to anything external"* and *"Absolute space, in its own nature, without regard to anything external, remains always similar and immovable"* were fundamental to Newtonian calculations. These Newtonian concepts of space and time were challenged and proven to be only approximate by Einstein through his 1905 paper on special relativity, as well as his discovery of general relativity in 1915.

According to Einstein (1920), the geometrical properties of space–time are dependent on the distribution of matter in space–time, so that if the accuracy of our calculations increases, small departures from the theory of Newton become apparent, though they may escape the test of our observations as these deviations are very small. In more modern terms, the geometrical properties of space–time (in particular the space–time metric g) are dependent and determined to some extent, through the field equation, by the distribution of mass-energy and mass-energy currents in space. It is now also true to say that, in many astrophysical systems, the departures from Newtonian predictions are not small, although these effects resort under the strong-field regime of general relativity theory (GRT), whereas space geodesy operates within the weak-field regime. The small

L. Combrinck (✉)
Space Geodesy Programme, Hartebeesthoek Radio Astronomy Observatory,
PO Box 443 Krugersdorp 1740, South Africa
e-mail: ludwig@hartrao.ac.za

deviations from Newtonian theory are also fundamental to experiments designed to evaluate general relativity in this weak-field regime.

Currently, the four main space geodetic techniques, Very Long Baseline Interferometry (VLBI), Global Navigation Satellite Systems (GNSS), Satellite or Lunar Laser Ranging (SLR/LLR) and Doppler Orbitography and Radiopositioning Integrated by Satellite (DORIS), have improved in accuracy to such an extent that for their optimal use one cannot disregard the effects of GRT. Analyses of the resulting data have to be done within the framework of a post-Newtonian formalism (Klioner 2003). In order to analyse the data correctly, the complete context within which the modelling is performed, i.e. reference and time frames, solar body ephemerides, signal propagation and observables (such as laser pulse travel time and satellite clock frequency) must consider GRT (Müller et al. 2008). These corrections are routinely done in advanced geodetic analysis software.

1.1 Introduction

In this chapter there is no space to describe the various space geodetic techniques in detail; however, the corrections and implications of GRT will be discussed in enough detail so as to allow practical application in software development, with adequate reference material for additional reading. Basically this chapter follows the recommendations of the international earth rotation service (IERS); see IERS Conventions (2003) (McCarthy and Petit 2003), IERS Conventions 2010 (Petit and Luzum 2010).

Solutions of GRT pertaining to space geodesy are weak-field, slow motion approximations. These approximations are valid as the gravitational field the solutions refer to has a potential U of small magnitude and the velocities v involved for any of the satellites are much less than the speed of light c. Therefore one has $U/c^2 \ll 1$ and $v/c \ll 1$ so that Einstein's field equations may be linearised and expressed in a form similar to Maxwellian equations of electromagnetism.

Space geodetic techniques depend to a large extent on the accuracy and stability of clocks; without these clocks the high accuracy measurements obtained currently would not be achieved. The timing aspect is therefore important and the high (atomic) clock accuracies have allowed an increase in measurement accuracy to such an extent that GRT must be applied to exploit the full potential of these techniques. A hydrogen maser clock is a requirement for VLBI (Wei-qun et al. 2001) with typical clock frequency accuracy of $\pm 5 \times 10^{-13}$ and stability of 9.7×10^{-15} in a 24 h period (geodetic VLBI experiments are normally of 24 h duration). Clock stability and accuracy are normally expressed in parts per so many counts; therefore a stability of 9.7×10^{-15} indicates that there are 9.7 excess counts for every 1×10^{15} counts or pulses in a 24 h period.

Apart from certain limitations (set by the atmosphere, spectral purity and stability of electronic equipment such as local oscillators and frequency multipliers),

the coherence time of a VLBI system is determined by the frequency standard, which normally acts as the fundamental frequency source for the other equipment.

The impact of clock phase stability can be seen in (2.1) which expresses VLBI signal to noise ratio:

$$\mathrm{SNR} = \frac{SA\sqrt{2B\tau_c}}{kT_s}. \tag{2.1}$$

In (2.1) the source density flux is denoted by S, the geometric mean of the telescope collecting areas is A, B is the bandwidth, τ_c is the coherent integration time, k is Boltzmann's constant and T_s is the geometric mean of the system temperatures of the radio telescopes (Moran 1989).

The coherent integration time τ_c is approximately

$$\omega \times \tau_c \times \sigma_y(T) = 1. \tag{2.2}$$

In (2.2) ω is the local oscillator frequency in radians per second and $\sigma_y(T)$ is the two-sample Allan variance. To provide an example, in order to achieve signal coherence for an observation period of 1,000 s, where the local oscillator frequency has been set to 8.0 GHz, the two frequency standards at each end of the interferometer need to maintain relative stability of $\sim 2 \times 10^{-14}$. As the observables in the VLBI technique are in principle recorded signals measured in the proper time of the station clocks, the influence of clock stability extends throughout the VLBI hardware.

In the IERS GRT model for VLBI time delay as amended 1 June 2004, (McCarthy and Petit 2003), the final result is kept accurate to picosecond level by including all terms of order 10^{-13} s or larger. The component of error in the total delay due to error in gravitational delay (~ 2 mm) is therefore a small fraction of the total delay error budget, especially in comparison to the total delay model's errors ascribed to the troposphere (~ 20 mm), radio source structure and antenna structure (~ 10 mm each) (Sovers et al. 1998). Therefore VLBI implementations of GRT corrections are currently at an appropriate level and their contribution to reduce the total modelling error is clear. The drive towards millimetre precision within the framework of the global geodetic observing system (GGOS) (see Beutler et al. 2005a in terms of historical motivation for GGOS) will require GRT modelling at <1 mm accuracy if its error contribution to the total is to remain proportionally small; GGOS aims for millimetre accuracy, so other error sources will have to be reduced by a factor of at least ten.

A main objective of GGOS is to improve dramatically our understanding of the implications of surface changes and mass transport and how these processes affect the dynamics of our planet. One of the main challenges of GGOS (Drewes 2007) is the combination of geometric and gravimetric methods in a common procedure, which will have to include consistent approaches, constants, conventions, models and parameters. Considering the complexity of the different techniques, processing software and independent research strategies, such a combination will have to be done without constraining independent and original model contributions, as this

could lead to scientific stagnation. As time observations are the basic observable in space geodesy, observations should be done using the same time system [e.g. Geocentric Coordinate Time (TCG—temps-coordonnée géocentrique)], and fundamental constants should be referred to the same time system. By implication a consistent GRT approach needs to be implemented in all space geodetic techniques to comply with and support the GGOS initiative.

1.2 Basic Implications of GRT for Space Geodesy Techniques

The basic effects of GRT on space geodetic measurements are related to how GRT affects the different observables and the dynamics of satellite orbits. Table 2.1 contains the main techniques and relativistic implications on their observables. Geometrically speaking, the Earth, Sun, Moon, planets and in fact all mass in the universe cause a curvature of space–time at some level in the immediate vicinity of the mass (in fact, in all the space–time). For instance, the curvature of space–time increases the up and down leg travel time of a laser pulse emitted by an SLR station to a satellite.

The effect on the main observable, time-of-flight (ToF), is an increase of several millimetres in the measured range (derived from the ToF) in the case of a LAGEOS satellite. In the case of near-Earth satellites, the effect of GRT can be modelled in the barycentric celestial reference system (BCRS) or geocentric celestial reference system (GCRS). Here we mainly consider the GCRS. The main relativistic effect on satellites in near-Earth orbit is due to the Schwarzschild field. Using LAGEOS as an example, the largest dynamical effect is the well known perigee advance, which for LAGEOS is ~ 9 mas/d (milli-arc-second per day).

Another smaller effect is the Lense–Thirring (frame dragging) effect (Lense and Thirring 1918), which causes a precession in the longitude of the ascending node (longitude of Ω) of ~ 31 mas/year (equal to about 1.8 m/year along-track displacement) and a change in the mean motion of a satellite. This precession is always in the direction of the rotation of the Earth. Frame dragging also advances the argument of perigee by ~ 31.6 mas/year. De Sitter (or geodesic) precession (de Sitter 1916) is due to the motion of the Earth through the gravitational field of the Sun and leads to a precession of the orbital plane of the satellite.

2 Satellite Laser Ranging

Satellite laser ranging (SLR) is introduced in Sciences of Geodesy I (Chap. 9). Considering SLR there are several GRT effects which need to be taken into account; these will be described in detail and examples of how they influence orbital determination will be given, using the LAGEOS satellites as ranging targets.

Table 2.1 GRT implications on space geodetic techniques

GRT effect	VLBI	GPS	SLR
Schwarzschild field		$3\frac{(GM)^2}{c^2a^3} = 2.8 \times 10^{-10}$ ms^{-2} $\Delta a = -4.4$ mm	(LAGEOS) $\dot\omega$ 9 mas/d $3\frac{(GM)^2}{c^2a^3} = 2.9 \times 10^{-9}$ ms^{-2} $\Delta a = -4.4$ mm
Lense–Thirring (frame dragging)		$2\frac{GM}{c^2a^2}nJ = 1.8 \times 10^{-12}$ m.s^{-2} $\Delta a/\cos i = -28$ μm $\dot\Omega = 8.8$ μas/d	$\dot\Omega \sim 31$ mas/year $\dot\omega \sim 31.6$ mas/year $2\frac{GM}{c^2a^2}nJ = 2.7 \times 10^{-11}$ ms^{-2} $\Delta a/\cos i = -42$ μm
de Sitter precession		$3\frac{GM_S}{c^2R}n_{San} = 2.28 \times 10^{-11}$ m.s^{-2} $\dot\Omega = 53$ μas/d	$3\frac{GM_S}{c^2R}n_{San} = 3.37 \times 10^{-11}$ m.s^{-2} $\dot\Omega \sim 17.6$ mas/year
Time-dilation, function of velocity		Onboard clock runs slow relative to a clock on the geoid −7.1 μs/day	
Amplitude of effect on clock at GPS satellite velocity of 3.874 km/s			
Gravitational red-shift (blue-shift), due to gravitational potential, function of altitude		Onboard clock runs fast relative to a clock on the geoid	
Amplitude of blue-shift at GPS orbital altitude of ~20 200 km		45.7 μs/day	
Combination of blue-shift and time-dilation		Satellite clock frequency must be reduced by 0.00455 Hz. GPS clock runs faster by 38.6 μs/days	

(continued)

Table 2.1 (continued)

GRT effect	VLBI	GPS	SLR
Additional contribution due to Earth's oblateness, amplitude of periodic effect		38 ps Peak to peak ~76 ps	
Additional contribution due to tidal potentials of Sun and Moon		Amplitude of periodic effect 1 ps	
Sagnac effect, depends on path and direction travelled (rotating frame of reference)		Onboard clock runs fast or slow relative to a clock on the geoid Maximum effect 136 ns	
Maximum effect for a stationary GPS receiver located on the geoid		133 ns	
Residual periodic effect at GPS orbital eccentricity of 0.02		Amplitude of residual periodic effect ~46 ns (Keplerian) peak to peak ~19 mm non-Keplerian <1.2 ns	
Shapiro delay	From 17×10^4 ps for a light ray grazing the Sun's limb to ~17 ps when the direction to the source is opposite to the Sun. Delay due to Earth's gravity field ~21 ps for a baseline of 6000 km	~19 mm	~7 mm
Gravitational light deflection	1.75 arcsec at limb of Sun (8.5 μrad)		

2.1 Shapiro Delay

Data obtained by the SLR system are converted to a normal point (NP) and by utilising the speed of light and incorporating some additional corrections; the Normal Point Range (NPR) can be calculated from the following:

$$\mathrm{NPR}_i = \frac{\left(\frac{\mathrm{NPtof}_i}{1\times 10^{12}} \times c\right)}{2} - \Delta a_i + \Delta CoM_i - \Delta R_{b_i} - \Delta GR_i - \Delta \varepsilon_i. \qquad (2.3)$$

In (2.3) the main observable NPtof_i is the normal point time-of-flight (in ps) at a certain epoch and c is (Kaplan 2005) the speed of light (299,792,458.0 m/s). The range given by the first term on the right-hand side of (2.3) needs to be corrected by taking into account the effects of the atmosphere Δa_i; subsequent terms are a satellite dependent centre-of-mass correction ΔCoM_i, SLR station range-bias ΔR_{b_i}, a relativistic correction (Shapiro 1964) (referred to as the Shapiro delay) ΔGR_i and other ($\Delta \varepsilon_i$) errors. If one uses LAGEOS as an example, the Shapiro delay correction is about 7 mm. According to McCarthy and Petit (2003),

$$t_2 - t_1 = \frac{\left|\overrightarrow{x}_2(t_2) - \overrightarrow{x}_1(t_1)\right|}{c} + \sum_J \frac{(1+\gamma)GM_J}{c^3} \ln\left(\frac{r_{J1} + r_{J2} + \rho}{r_{J1} + r_{J2} - \rho}\right). \qquad (2.4)$$

In (2.4), γ is the parameterised post-newtonian (PPN) (Eddington 1923; Robertson 1962) parameter which should equal unity if GRT is valid, $t_2 - t_1$ denotes the total time delay considering a laser pulse emitted from coordinate x_1 (SLR station) at time t_1 and the return pulse is received at coordinate x_2 (SLR station) at time t_2. The PPN formalism (Will and Nordtvedt 1972) is a framework designed to classify various theories of gravity according to five attributes, which include curvature of space–time and nonlinearity of gravity. This formalism is valuable in tests and evaluations of GRT. In (2.4) the range defined by $\rho = \left|\overrightarrow{x_2} - \overrightarrow{x_1}\right|$ is the uncorrected (for GRT) range; in addition $r_{J1} = \left|\overrightarrow{x_1} - \overrightarrow{x_J}\right|$ and $r_{J2} = \left|\overrightarrow{x_2} - \overrightarrow{x_J}\right|$. This formulation was first derived by Holdridge (1967), which was a more elegant solution than previous solutions which involved angles. The last term in (2.4) describes the (Shapiro) correction for space curvature. Similar to the calculation of the numerator of the first term in (2.4), determination of the relativistically uncorrected range ρ is not simply the subtraction of two vectors, but involves an iterative solution of two light-time equations for the uplink and downlink path. This procedure is described in Montenbruck and Gill (2001) and Combrinck (2010). For the upleg (SLR station to satellite) a fixed-point iteration with

$$\tau_u^{(i+1)} = 1/c \cdot \left|\vec{r}(t - \tau_d) - \vec{R}\left(t - \tau_d - \tau_u^{(i)}\right)\right| \qquad (2.5)$$

is executed in a loop until τ_u achieves an accuracy threshold that has been defined in the software algorithm. Four to five iterations are normally adequate. All calculations are done in an inertial (geocentric) reference frame (for example J2000).

Considering the downleg, the initial condition is $\tau_0 = 0$, then consecutive solutions are done using the fixed-point iteration

$$\tau_d^{(i+1)} = 1/c \cdot \left| \vec{r}(t - \tau^i) - \vec{R}(t) \right|. \tag{2.6}$$

The average of upleg range ρ_u and downleg range ρ_d, can then be used to find the range $\rho = \left| \vec{x_2} - \vec{x_1} \right|$ in (2.4) where

$$\rho = 0.5(\rho_u + \rho_d). \tag{2.7}$$

In the formulation given by (2.4), the sum is carried over all bodies J with mass M_J centred at x_J (McCarthy and Petit 2003). In practice, only the Earth needs to be considered as J for near-Earth satellites (including LAGEOS), as analysis is done in the geocentric frame of reference (Ries et al. 1988; Huang et al. 1990).

2.2 GRT Accelerations

A satellite experiences a variety of accelerations when in orbit and accelerations due to GRT can be separated from those that are purely Newtonian (at least in the weak-field and slow motion regime). One can therefore write the perturbing acceleration as

$$\ddot{\vec{r}} = -\frac{GM_\oplus}{r^3} \vec{r} + \vec{f}, \tag{2.8}$$

where (extending the notation of Tapley et al. 2004) the total perturbing force $\vec{f}$ is made up of a number of additional forces which perturb the orbit in addition to the first term in (2.8), which can be written as

$$\vec{f} = \vec{f}_{NS} + \vec{f}_{TC} + \vec{f}_{3B} + \vec{f}_g + \vec{f}_{Drag} + \vec{f}_{SRP} + \vec{f}_{ERP} + \vec{f}_{other} + \vec{f}_{Emp} \tag{2.9}$$

In (2.9) $\vec{f}_{NS}$ results from the uneven Earth mass-distribution, while the temporal variations of the static gravity field are represented by $\vec{f}_{TC}$. Perturbations caused by the gravitational forces from the Sun, Moon and planets are denoted by $\vec{f}_{3B}$, GRT is described by $\vec{f}_g$, atmospheric drag is $\vec{f}_{Drag}$, $\vec{f}_{SRP}$ is due to solar radiation, $\vec{f}_{ERP}$ is the Earth radiation pressure and $\vec{f}_{Other}$ contains other (very small) forces such as thermal, satellite rotation dependent effects. Once per-cycle-per-revolution empirical corrections, usually expressed in a local frame and divided into radial, tangential and normal (RTN) components are given by $\vec{f}_{Emp}$. A brief discussion of these perturbing forces is made in Book I (Chap. 9) of this series. Additional discussions can be found in the literature (cf. Hoffman-Wellenhof and Moritz 2005).

The IERS 2003 (McCarthy and Petit 2003) recommendations discuss the relativistic correction to the acceleration of a satellite in Earth orbit where

$$\Delta \vec{r} = \frac{GM_\oplus}{c^2 r^3} \left\{ \left[2(\beta + \gamma) \frac{GM_\oplus}{r} - \gamma \left(\dot{\vec{r}} \cdot \dot{\vec{r}} \right) \right] \vec{r} + 2(1 + \gamma) \left(\vec{r} \cdot \dot{\vec{r}} \right) \dot{\vec{r}} \right\}$$

$$+ (1 + \gamma) \frac{GM_\oplus}{c^2 r^3} \left[\frac{3}{r^2} \left(\vec{r} \times \dot{\vec{r}} \right) \left(\vec{r} \cdot \vec{J} \right) + \left(\dot{\vec{r}} \times \vec{J} \right) \right] \qquad (2.10)$$

$$+ \left\{ (1 + 2\gamma) \left[\dot{\vec{R}} \times \left(\frac{-GM_s \vec{R}}{c^2 R^3} \right) \right] \times \dot{\vec{r}} \right\}$$

is the correction which includes as:

- First term, the nonlinear Schwarzschild field of the Earth $(\approx 10^{-9}\,\mathrm{m\,s^{-2}})$
- Second term, Lense–Thirring precession (frame dragging) $(\approx 10^{-11}\,\mathrm{m\,s^{-2}})$
- Third term, de Sitter (geodesic) precession $(\approx 10^{-11}\ \mathrm{m\,s^{-2}})$

Equation (2.10) is due to the formalism of Damour et al. (1994).

In (2.10), the speed of light is denoted by c, and PPN parameters β, γ equal unity if general relativity is valid. The parameter β (Eddington 1923; Robertson 1962) questions how much nonlinearity there is in the superposition law for gravity (refer to Will and Nordtvedt 1972 for a modern description of PPN parameters). The position of the satellite relative to the Earth is $\vec{r}$ and $\vec{R}$ is the position of the Earth relative to the Sun. Earth's angular momentum per unit mass is described (Petit and Luzum 2010) by $\left| \vec{J} \right| \cong 9.8 \times 10^8\ \mathrm{m^2 s^{-1}}$, $GM_\oplus$ is the gravitational coefficient of Earth (also μ in this chapter or GM) and GM_s the gravitational coefficient of the Sun.

Although these accelerations are small, they must be included for precise orbit determination (POD) purposes as there are some long term periodic and secular effects (Huang and Liu 1992) of the orbit. Precession of perigee results from the Schwarzschild effect, de Sitter precession can lead to long-period variations of some orbital elements (Ω, ω, M) and Lense–Thirring precession leads to secular rates (Ciufolini and Wheeler 1995) in the orbital elements Ω and ω. Refer to Table 2.1 for comparative rates between GNSS and LAGEOS.

Following Hugentobler (2008), it is quite informative to have a closer look at the separate terms of (2.10) in more detail, which will be done in the following sections for the three relativistic components. The Gaussian perturbations of a satellite orbit (Beutler et al. 2005b; Xu 2007) is given by (cf. Vallado 2001, for a discussion on limitations of the Gaussian form of the variation of parameters)

$$\dot{a} = \sqrt{\frac{p}{GM}} \frac{2a}{1 - e^2} \left[e \sin v \cdot R + \frac{p}{r} \cdot S \right], \qquad (2.11)$$

$$\dot{e} = \sqrt{\frac{p}{GM}} [\sin v \cdot R + (\cos v + \cos E) \cdot S], \qquad (2.12)$$

$$\dot{i} = \frac{r \cos u}{na^2 \sqrt{1 - e^2}} \cdot W, \tag{2.13}$$

$$\dot{\Omega} = \frac{r \sin u}{na^2 \sqrt{1 - e^2} \sin i} \cdot W, \tag{2.14}$$

$$\dot{\omega} = \frac{1}{e} \sqrt{\frac{p}{GM}} \left[-\cos v \cdot R + \left(1 + \frac{r}{p}\right) \sin v \cdot S \right] - \dot{\Omega} \cos i, \tag{2.15}$$

$$\dot{M}_0 = \frac{1 - e^2}{nae} \left[\left(\cos v - 2e\frac{r}{p}\right) \cdot R - \left(1 + \frac{r}{p}\right) \sin v \cdot S \right] - \frac{3n}{2a}(t - t_0)\dot{a}. \tag{2.16}$$

Here a is the semi-major axis, v is the true anomaly, u is the argument of latitude and the argument of perigee is denoted by ω. The distance from the primary focus to the orbit (semiparameter, also known as "semi-latus rectum") is given by $p = a(1 - e^2)$ and the average angular velocity is described by

$$n = \frac{2\pi}{T} = a^{-3/2}\mu^{1/2}, \tag{2.17}$$

where $\mu = GM$ and the period of the satellite motion T can be written (Xu 2007) as

$$T = \frac{\pi ab}{\frac{1}{2}h} = \frac{2\pi ab}{\sqrt{\mu a (1 - e^2)}} = 2\pi a^{0.7ex3/2}\mu^{-0.7ex1/2}. \tag{2.18}$$

Considering secular perturbations and circular orbits $(e = 0)$, the radial (R), along-track (S) and cross-track (W) perturbing accelerations are directed parallel to the vectors $\vec{r}, \dot{\vec{r}}$ and $\vec{r} \times \dot{\vec{r}}$ respectively. For non-circular orbits the along-track axis (S) is not parallel (except at perigee and apogee) to the velocity vector. During processing, the position and velocity vectors of a satellite (including gravity gradients etc.) are normally transformed into an inertial reference frame such as ICRF/EME2000. The position, velocity and angular momentum vectors can then be written in a frame with the z axis orthogonal to the orbital plane as

$$\begin{aligned} \vec{r} &= a(\cos v, \sin v, 0) \\ \vec{v} &= an(-\sin v, \cos v, 0) \\ \vec{r} \times \vec{v} &= a^2 n(0, 0, 1). \end{aligned} \tag{2.19}$$

The unit vectors (direction vectors) of the perturbing accelerations can be written as

$$\begin{aligned} \hat{e}_R &= (\cos v, \sin v, 0) \\ \hat{e}_S &= (-\sin v, \cos v, 0) \\ \hat{e}_W &= (0, 0, 1). \end{aligned} \tag{2.20}$$

2.2.1 Nonlinear Schwarzschild Field Contribution to Acceleration

The first term of (2.10) is the contribution of the Schwarzschild metric (static part of the field generated by the central mass) to the GRT acceleration. Schwarzschild (1873–1916) was a German astrophysicist who found the first rigorous solution of Einstein's field equations. This solution is suitable (to a good approximation) for application to satellites in orbit around Earth. His original paper (Schwarzschild 1916) utilises as a background theme the excess beyond pure Newtonian motion of the perihelion of Mercury. While located at the Russian front, Karl Schwarzschild solved this problem by taking into account Einstein's requirements for a solution to the motion of the perihelion of Mercury. Consequently he found the solution to "the line element that forms the exact solution of Einstein's problem" and continued to derive the motion of a point in the gravitational field, i.e. the geodesic line corresponding to the line element.

When a topological space is described locally by Euclidean geometry, it is a manifold. In the immediate vicinity of a point in the manifold, there is a neighbourhood of points which is nearly flat. This reminds one that all statements regarding the principle of equivalence are *local* in nature. Einstein's solution of the Mercury perihelion problem was only to first order, whereas Schwarzschild's solution was exact. Mercury's total observed perigee advance is 574 arcsec per century, mostly due to planetary gravitational perturbations. The excess is about 43 arcsec, in agreement with GRT; this was one of the first 'proofs' of the validity of GRT. In space geodesy, when considering satellite orbits in the immediate vicinity of Earth (including high Earth orbiters such as GLONASS and GPS), it is convenient to use the Schwarzschild geometry as Earth's gravity field model even though it excludes the rotational effect of Earth in the gravity field. The metric of a space is basically its distance measure. Considering the metric of the Schwarzschild geometry (static spherically symmetric geometry), it has the form

$$\mathrm{d}s^2 = -\left(1 - \frac{2GM}{rc^2}\right)c^2\mathrm{d}t^2 + \left(1 - \frac{2GM}{rc^2}\right)^{-1}\mathrm{d}r^2 + r^2\mathrm{d}\theta^2 + r^2\sin^2\theta\mathrm{d}\phi^2. \quad (2.21)$$

This form (Schwarzschild coordinates) is only simple when unperturbed and unmodified; furthermore it is not in isotropic coordinates (Misner et al. 1973). In (2.21) the universal gravitational constant is denoted by G, and M is a parameter with dimensions of mass, which for our purposes is the mass of Earth. The quantity s is the proper time in seconds, r is the radial coordinate in metres, t is the time coordinate in seconds, θ is the colatitude and ϕ is the longitude (both in radians). If M was set to zero, the result would be equal to the Minkowskian (gravity-free space–time) four-dimensional metric expressed in spherical polar spatial coordinates. Minkowski space is recovered when $M/r \to \infty$.

The Schwarzschild line element can be modified to isotropic coordinates so that the relationship between r, θ, ϕ and x, y, z can be described in the usual manner, with $r = (x^2 + y^2 + z^2)$ becoming an isotropic coordinate [see (2.85) and (2.86)],

which should not be confused with r in the Schwarzschild coordinates (see Misner et al. 1973).

Experimental confirmation during the last 3 centuries using optical instruments and radar observations since 1966 has provided credibility for GRT theory. Some polemic still surrounds the issue, as several other parameters could also affect the exact value of the advance, e.g. the quadrupole, J_2, which is not yet very accurately determined, contribution of the Sun as well as the (small) gravitomagnetic contribution resulting from the angular momentum of the Sun. A detailed account of the drama surrounding the initial proof and resistance to acceptance of GRT can be found in Crelinsten (2006) and more technical details can be obtained from Ciufolini and Wheeler (1995).

Following Hugentobler (2008), if we set $GM = n^2 a^3$ the Schwarzschild acceleration for a circular orbit can be written as

$$
\begin{aligned}
\Delta \vec{r}_S &= \frac{GM}{c^2 a^3} \left[4 \frac{GM}{a} - v^2 \right] \vec{r} \\
&= \frac{GM}{c^2 a^3} \left[4 \frac{GM}{a} - \frac{GM}{a} \right] \vec{r} \\
&= 3 \frac{(GM)^2}{c^2 a^4} \cdot \vec{r}.
\end{aligned}
\tag{2.22}
$$

The radial component of the Schwarzschild acceleration is then

$$
R = \vec{e}_R \cdot \Delta \vec{r}_S = 3 \frac{(GM)^2}{c^2 a^3},
\tag{2.23}
$$

whereas the alongtrack and crosstrack accelerations are both equal to zero:

$$
S = \vec{e}_S \cdot \Delta \vec{r}_S = 0 \quad \text{and} \quad W = \vec{e}_W \cdot \Delta \vec{r}_S = 0.
\tag{2.24}
$$

Considering the sign convention of gravitational acceleration as per (2.8) it is clear that the radial component of the Schwarzschild field imparts an outward acceleration, which reduces the Newtonian component, effectively changing GM so that

$$
\begin{aligned}
\vec{e}_R \cdot \vec{r}_{\text{tot}} &= -\frac{GM}{a^2} + R \\
&= -\frac{GM}{a^2} \left(1 - \frac{Ra^2}{GM} \right) \\
&= -\frac{GM'}{a^2}.
\end{aligned}
\tag{2.25}
$$

Using Kepler's third law written as (2.17) where $\mu = GM$ and keeping the period T of the satellite motion (2.18) fixed and setting $a' = a + \Delta a$, then

$$
a'^3 n^2 = GM'
\tag{2.26}
$$

and to first order

$$\Delta a = -\frac{1}{3}\frac{Ra^3}{GM}. \tag{2.27}$$

Substituting R from (2.23) into (2.27) one can then write (Hugentobler 2008)

$$\Delta a = -\frac{GM}{c^2} = -4.43 \text{ mm}. \tag{2.28}$$

The Schwarzschild acceleration on a satellite in orbit is thus a radial, in-plane effect, with zero magnitude effects in the alongtrack and crosstrack directions.

2.2.2 Lense–Thirring Precession

The second term of (2.10) is due to Lense–Thirring precession; it is clear that the Earth's angular momentum J plays a major role in the generation of the Lense–Thirring effect. In the case of LAGEOS, the effect is very small (~ 31 mas/year) and is therefore extremely difficult to measure (Ciufolini 1986). The secular rates of the ascending node and perigee of a body orbiting a central rotating mass is given by (Lense and Thirring 1918)

$$\dot{\Omega}_{\mathrm{LT}} = \frac{2GJ}{c^2 a^3 (1 - e^2)^{3/2}} \tag{2.29}$$

and

$$\dot{\omega}_{\mathrm{LT}} = -\frac{6GJ \cos i}{c^2 a^3 (1 - e^2)^{3/2}}, \tag{2.30}$$

where G is the gravitational constant, c denotes the speed of light, J is the proper angular momentum of Earth, and a, e and i are the semi-major axis, eccentricity and inclination of the orbit respectively. Following Hugentobler (2008) the angular momentum vector can be written in the reference frame as defined by (2.19) as

$$\vec{J} = J(0, \sin i, \cos i). \tag{2.31}$$

In the case of a circular orbit, therefore,

$$\vec{r} \cdot \vec{J} = aJ \sin i \sin v \text{ and } \vec{r} \times \vec{J} = anJ(\cos v \cos i, \sin v \cos i, -\sin v \sin i). \tag{2.32}$$

The radial, alongtrack and crosstrack components are then

$$R = \Delta \vec{r}_{LT} \cdot \vec{e}_R = 2\frac{GM}{c^2 a^4}\vec{r} \cdot \left(\vec{r} \times \vec{J}\right) = 2\frac{GM}{c^2 a^4}\vec{J} \cdot \left(\vec{r} \times \vec{r}\right) = 2\frac{GM}{c^2 a^2} nJ \cos i, \tag{2.33}$$

$$S = \Delta \vec{r}_{LT} \cdot \vec{e}_S = 0, \tag{2.34}$$

$$W = \Delta \vec{r}_{LT} \cdot \vec{e}_W$$
$$= 2 \frac{GM}{c^2 a^3} \left[\frac{3}{a^2} a^2 naJ \sin i \sin v - anJ \sin i \sin v \right] \tag{2.35}$$
$$= 4 \frac{GM}{c^2 a^2} nJ \sin i \sin v.$$

The semi-major axis undergoes a reduction of

$$\Delta a = -\frac{2}{3} \frac{anJ}{c^2} \cos i \propto a^{-1/2}, \tag{2.36}$$

due to the constant radial acceleration. If the orbit is perpendicular to the equatorial plane there is no radial acceleration or change in semi-major axis due to the $\cos i$ factor in (2.36). Changes in the semi-major axis are inversely proportional to the square root of the semi-major axis, so that higher orbit satellites experience a smaller effect.

Considering (2.14) and setting $u = v$ (true anomaly is undefined for circular orbits as they have no periapsis) in the case of a circular orbit,

$$\dot{\Omega}_{LT} = \frac{\sin u}{na \sin i} \cdot W$$
$$= 4 \frac{GM}{c^2 a^3 J \sin^2 u} \tag{2.37}$$
$$= 2 \frac{GM}{c^2 a^3 J (1 - \cos 2u)}.$$

The precession of the node is not dependent on the inclination i of the orbit as it is a frame precession effect; it is inversely related to a^3 so that it decreases very rapidly. Iorio (2007) provides an alternative discussion on the (RTN) radial($\vec{r}$), transverse ($\vec{t}$) and out-of-plane ($\vec{n}$) projections of the perturbing acceleration, commencing with the Gaussian perturbation equations of a satellite orbit.

2.2.3 de Sitter (Geodesic) Precession

Geodesic precession is basically a result of the motion of Earth through the Sun's gravitational field. The consequences are that a satellite's orbital pole precesses about the normal to the ecliptic at a rate of 19.2 milliarcseconds (mas) per year and the ascending node of the satellite's orbit on the ecliptic increases in celestial longitude by 19.2 mas per year (Moyer 2000). In addition, geodesic precession decreases the general precession by 19.2 mas.

Both de Sitter precession and Lense–Thirring precession are manifestations of frame-dragging as clearly shown by Ashby and Shahid-Saless (1990). Within an appropriately chosen coordinate system and without incorporating spatial curvature, geodetic precession of a gyroscope orbiting a spherically symmetric, spinning mass can be remoulded as a Lense–Thirring frame-dragging effect. Geodesic

precession and Lense–Thirring precession can therefore be described in terms of two components of a single gravitomagnetic effect. As applied to SLR, the Lense–Thirring component is due to the spin angular momentum of Earth whereas the deSitter precession can be ascribed to the orbital angular momentum of Earth as it revolves around the origin of the appropriately selected quasi-inertial coordinates. This interpretation is still a matter of debate however, (cf. Ciufolini and Wheeler 1995; Ciufolini 2007) where some interpretations regard the de Sitter effect and the Lense–Thirring drag as fundamentally different phenomena.

Following Hugentobler (2008), in curved space–time, a parallel transported (local inertial) reference frame undergoes precession with respect to distant stars. For a satellite the precession rate (19.2 mas/year in the vicinity of Earth) does not depend on the distance from the Earth. The equation describing the resulting acceleration [refer to (2.10)] is

$$\Delta \vec{\ddot{r}}_{dS} = -2 \left[-\frac{3}{2} \frac{GM_S}{c^2 R^3} \vec{R} \times \vec{\dot{R}} \right] \times \vec{r}. \tag{2.38}$$

Equation (2.38) has the form of a Coriolis term. The Coriolis acceleration of a satellite in orbit around the Earth due to geodesic precession is

$$\ddot{\vec{r}} = 2\vec{\Omega} \times \dot{r}, \tag{2.39}$$

where the angular velocity vector due to geodesic precession (Moyer 2000) is

$$\vec{\Omega} = \frac{GM_S \left(\gamma + \frac{1}{2}\right)}{c^2 R^3} \left(\vec{R} \times \vec{\dot{R}} \right). \tag{2.40}$$

The formulations at (2.39) and (2.40) [instead of (2.38)] are useful if the PPN parameter γ needs to be included in an estimation process and is equivalent to the third term of (2.10). In (2.38) M_S is the mass of the Sun and R is the distance to it, respectively. The precession vector $\vec{\omega}_{dS}$ of the global frame (the term in brackets) is relative to the precessing (local inertial) frame and it points to the southern ecliptic pole. If the frame defined in (2.19) is redefined by keeping the z-axis the same but rotating the x-axis towards the ascending node with respect to the ecliptic plane (Hugentobler 2008), the precession vector of the global frame can be written as

$$\begin{aligned} \vec{\omega}_{dS} &= -\frac{3}{2} \frac{GM_S}{c^2 R^3} \vec{R} \times \vec{\dot{R}} \\ &= -\frac{3}{2} \frac{GM_S}{c^2 R} \sqrt{1 - e_S^2} n_S (0, \sin \beta, \cos \beta). \end{aligned} \tag{2.41}$$

In (2.41) the mean motion of Earth around the Sun is denoted by n_S and the inclination of the orbital plane to the ecliptic is represented by β. The inclination is in the range $(i - \varepsilon, i + \varepsilon)$ and can be calculated using

$$\cos \beta = \cos \varepsilon \cos i + \sin \varepsilon \sin i \cos \Omega, \tag{2.42}$$

with the obliquity of the ecliptic $\varepsilon = 23°26'$. In the defined frame, for a circular orbit the relation

$$\left(\vec{R} \times \dot{\vec{R}}\right) \times \vec{r} = R^2 n_S \sqrt{1 - e_S^2} \, an \left(-\cos \beta \cos v, -\cos \beta \sin v, \sin \beta \sin v\right),$$
(2.43)

can be written and consequently (Hugentobler 2008) the perturbing accelerations are

$$R = \Delta \vec{r}_{dS} \cdot \vec{e}_R = -3 \frac{GM_S}{c^2 R} n_S \sqrt{1 - e_S^2} an \cos \beta, \tag{2.44}$$

$$S = \Delta \vec{r}_{dS} \cdot \vec{e}_S = 0, \tag{2.45}$$

$$W = \Delta \vec{r}_{dS} \cdot \vec{e}_W = 3 \frac{GM_S}{c^2 R} n_S \sqrt{1 - e_S^2} an \sin \beta \sin v. \tag{2.46}$$

Considering the $\cos \beta$ factor in the radial component, orbits which are perpendicular to the ecliptic plane experience no change in semi-major axis and no radial acceleration as the Coriolis acceleration is perpendicular to the orbital plane.

The negative radial acceleration increases the semi-major axis by

$$\Delta a = +\frac{GM_S}{c^2} \frac{a}{R} \frac{n_S}{n} \sqrt{1 - e_S^2} \cos \beta \propto a^{5/2}. \tag{2.47}$$

Using (2.14) and setting $u = v$ for a circular orbit the precession of the ascending node with respect to the ecliptic plane can be calculated as

$$\begin{aligned}
\dot{\Omega}_{dS} &= \frac{\sin u}{na \sin \beta} \cdot W \\
&= 3 \frac{GM_S}{c^2 R} n_S \sqrt{1 - e_S^2} \sin^2 u \\
&= 3 \frac{GM_S}{c^2 R} n_S \sqrt{1 - e_S^2} s(1 - \cos 2u).
\end{aligned} \tag{2.48}$$

Figure 2.1 illustrates the acceleration values of the radial components of the three terms of (2.10), as described by (2.23, 2.33) and (2.44). Considering LAGEOS, the acceleration due to the radial component of the de Sitter effect is slightly larger than the component due to the frame-dragging effect. The Lense–Thirring effect dominates the de Sitter effect for semi-major axes that are less than 11,000 km. Table 2.1 summarizes some of the relativistic accelerations and advances of perigee and the node due to the three terms of (2.10).

According to the IERS Conventions 2010 (Petit and Luzum 2010), the magnitude and observable effects of these relativistic components depend to some extent on the satellite orbital characteristics and the analysis setup strategy. For instance, the satellite height changes during its orbital path so that $a \simeq r$ for near circular orbits, so the slightly simplified examples here for circular orbits will provide slightly different answers compared to a rigorous implementation of (2.10),
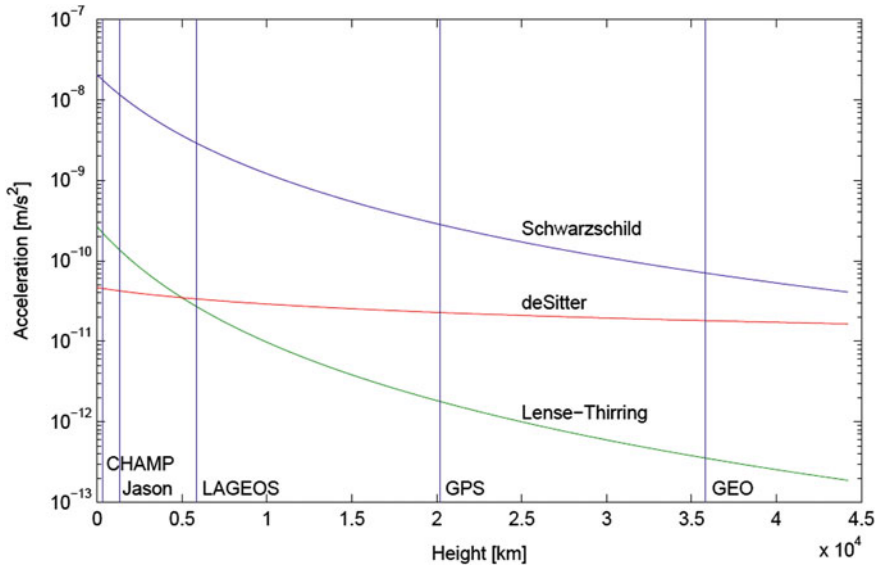
Fig. 2.1 Radial acceleration as a function of satellite height for circular orbits (Hugentobler 2008)

even though LAGEOS and GPS satellites have very nearly circular orbits. If (as suggested by Petit and Luzum 2010) orbital parameters are adjusted and the Schwarzschild term is not taken into account, there would be an apparent 4.4 mm decrease in orbital radius as described using the formulations of Hugentobler (2008). This stresses the necessity for consistent application of the formulation at (2.10), as different strategies (and different values of, for instance, the Earth's angular momentum per unit mass) will lead to different results.

2.3   SLR Tests of General Relativity Theory

In the immediate environment of our solar system, the linearised weak-field and slow-motion approximation is adequate and is the regime where space geodesy can be utilised to test GRT. As mentioned by Einstein (1920), these deviations beyond pure Newtonian dynamics *may escape the test of our observations* as these deviations are very small. This certainly is still the case to some extent, as experiments designed to test GRT are often very difficult and expensive. For example, the next higher accuracy tests are likely to come from GAIA (a space-based astrometric mission). The GAIA mission (Turon et al. 2005) has as its objective the creation of a three-dimensional map of our galaxy, which will improve our knowledge of its composition, formation and evolution. In addition, new tests of general relativity are included in its projected five-year mission, with a

launch date currently estimated for 2013. Estimated accuracy for the evaluation of PPN parameter γ with GAIA is $\sim 2 \times 10^{-7}$ (Vecchiato et al. 2003). Estimated angular accuracy [this is a best scenario case as this accuracy is a function of magnitude and ecliptic latitude of the object (Lindegren 2009)] is $\leq 10 \,\mu\text{as}$ (Perryman et al. 2001), which is a factor of ten or more better than what is (currently) routinely achieved with VLBI. Included in its mission objectives are tests for light deflection, time delay, and Doppler frequency shift as well as perihelion precession. Even though missions such as these will constantly be added to the list of attempts to improve the accuracy of GRT tests (Turyshev 2009), space geodesy has its own role to play; for instance, SLR can be used to measure frame dragging, gravitational delay, and can also be used to estimate PPN parameters γ and β.

2.3.1 Tests of Frame Dragging (Lense–Thirring Effect)

SLR has been used in attempts to detect frame dragging. Using SLR and the LAGEOS satellite to detect frame dragging was initially proposed by Cugusi and Proverbio (1977), see also Cugusi and Proverbio (1978). The first reported results were by Ciufolini et al. (1996) who analysed the SLR range observations of satellites LAGEOS and LAGEOS II utilising the software package GEODYN II (Pavlis et al. 2007). They obtained the first direct measurement of the Lense–Thirring effect, or dragging of inertial frames, and the first direct experimental evidence for the gravitomagnetic field. The stated accuracy of their measurement was $\sim 30\%$. This work was very valuable in that it created opportunity for more investigation using improved gravity models and higher accuracy perturbation models; it also started a competitive and critically evaluated research avenue.

   This first report was followed by Ciufolini et al. (1998), claiming an improved result of 20%; the parameter μ is introduced, which measures the strength of the Lense–Thirring effect (in GRT, $\mu \equiv 1$). Initially both nodes of LAGEOS I and II were used as well as the argument of perigee of LAGEOS II. Satellite LAGEOS I has a smaller eccentricity (~ 0.004) than LAGEOS II (~ 0.14), which makes detection of the advance in the argument of perigee of LAGEOS I more difficult, and in addition the frame dragging effect is nearly twice the value for LAGEOS II than for LAGEOS I.

   Subsequent estimates used only the nodes (Ciufolini and Pavlis 2004, Ciufolini et al. 2006) in a 'butterfly' configuration of the retrograde LAGEOS I ($i = 109.8°$) and the prograde LAGEOS II ($i = 52.6°$) orbits. A very dedicated effort to create a realistic error budget is contained within the Ciufolini et al. (2006) paper, where several gravity models are used. Best estimates were obtained by using the EIGEN-GRACE02S model, where $\mu = 0.99$, with a total error between 5 and 10% of the GRT predicted value of the Lense–Thirring effect. The improved results are directly related to the improved gravity models, as the frame dragging tests can be strongly affected by mismodelling of the even zonal harmonic coefficients. Other sources of error which have a smaller impact result from model imperfections of

any factor which causes orbit perturbations including the solid Earth and pole tides as they modulate the static gravity field.

The results of the most recent SLR-based tests in determining frame dragging using the LAGEOS satellites have been questioned by Iorio (2010b). The contributions by Iorio are important in that a careful scrutiny of the techniques employed, evaluation of error sources, and independent tests are necessary to ensure that results are scientifically valid. These tests are not trivial as the small effects which are being investigated are easily obscured by classical phenomena which are explained in Newtonian terms. According to Iorio (2010b), the systematic error $\delta\mu$ in the Lense–Thirring measurements published to date should be increased by a factor of 3–4 times. Following the literature, a healthy debate has developed and continues regarding these tests and there are numerous publications concerning the validity of these tests (Iorio 2006). The effect of Iorio's work has been that much more attention has been given to evaluation of the magnitude and influence of errors on estimates of frame dragging.

2.3.2 Estimation of Perigee Shift in the Schwarzschild Gravitoelectric Field

In the previous section we had a glimpse of the activities of researchers determining the effects of gravitomagnetism. The general relativity shift of the perigee of LAGEOS II resulting from the Schwarzschild gravitoelectric field has been estimated by Lucchesi (2003) during a simulation of a measurement and error budget. Using the gravity model EGM96, Lucchesi demonstrated the potential to estimate LAGEOS II's general relativistic shift with 2% accuracy. Error budget estimation covered an observational period of approximately 7 years. Similar to the determination of frame dragging due to gravitomagnetism, the largest errors are due to the uncertainties in the even zonal harmonics of the Earth's gravity field and to a lesser extent the mismodelling of non-gravitational perturbations. The result obtained may be viewed as a 2% accuracy derivation of the PPN parameters γ and β. Details of error sources and their possible influence are given.

2.3.3 Estimation of Perigee Shift in the Schwarzschild Gravitoelectric and Gravitomagnetic Field

A very interesting approach was taken recently by Lucchesi and Peron (2010), placing moreover new constraints on non-Newtonian gravity. They analysed 13 years of SLR data of the LAGEOS satellites with the GEODYN II (Pavlis et al. 2007) software; the models for general relativity were not included in the orbit determination, thereby obtaining the relativistic signal in the residuals. Utilising LAGEOS II pericentre residuals they were able to obtain a 99.8% agreement with the predictions of Einstein's theory. Basically this approach is a measurement in the field of the Earth of the combination of the γ and β PPN parameters of general

relativity. This work is different from other approaches as it measures all the relativistic secular effects simultaneously. It is unfortunately not able to separate the PPN parameters γ and β, as this result, essentially from the "Schwarzschild" signal, places a constraint only on the combination of γ and β. Other, separate constraints would be required to disentangle them. The signals from the Lense–Thirring and de Sitter components could provide information on γ, but their signal-to-noise ratios in the case of LAGEOS I are too small to be really useful in this respect (Peron, 3 Mar 2011, "personal communication"). This unique approach in the PPN framework can be considered as a 0.03% measurement of the combination of γ and β PPN parameters. The results of Lucchesi and Peron (2010) also constrain possible deviations from the gravitational inverse-square law in favour of new weak interactions parameterised by a Yukawa-like potential with strength α and range λ.

2.3.4 Direct Estimates of PPN Parameters

The estimation of PPN parameters γ and β can be done directly within the least-squares solution of precise orbital determination. A first attempt was undertaken by Combrinck (Combrinck 2008), providing an error of $\sim 5 \times 10^{-4}$ on γ. In these tentative initial results, the PPN parameter was evaluated as a solve-for parameter in an analysis of five months of LAGEOS II SLR data. A rejection filter was used to constrain the orbital integration and parameter estimation. However, it was noted that careful analyses of the effects of alternative strategies such as different gravity models and a priori constraints on other solve-for or consider parameters need to be done to evaluate this technique. The consider parameters are parameters which could be estimated, but by setting their a priori constraints very high (i.e. very low error values), they essentially obtain fixed values but are affected by their uncertainties. This evaluation includes the Schwarzschild terms and the effects of rotational frame-dragging (Lense–Thirring precession), de Sitter (geodesic) precession and Shapiro delay. The solved for PPN parameters are fed back into the least-squares process during the analysis.

In this approach, the radial component of the SLR measurements is the strength of the technique; the relativistic acceleration on LAGEOS is mainly a radial component. This preliminary study solved for γ in the least-squares sense utilising SLR data in a strategy where the O–C residuals indicate better observation/ modelling fits, through different levels of O–C residual rejection levels. This strategy assigns greater weight to SLR measurement accuracy than to the modelling parameters. Basically the filter consists of low-pass and high-pass criteria set to an O–C standard deviation based on a selected number of iterations during the least-squares fitting process. This effectively creates a bandpass filter, which rejects observations which fall outside the rejection criteria level.

Additional work done since included estimates of both γ and β using a longer time series of ~ 4 years (Combrinck 2011). In this work, the suggestion by Iorio (2010a) that possible imprinting of GRT in the gravity field models could adversely affect tests of GRT is taken into account. Therefore certain gravity field

spherical harmonic coefficients, $J_2 - J_5$, C_{21} and S_{21}, are estimated. This requires a step by step approach where currently 20 iterations in the least-squares solution are required, with certain parameters being estimated at certain iterations. Coefficients C_{21} and S_{21} together with J_2 are estimated to determine pole tide. In comparison to γ the estimate for β is weaker using this technique, as β is only evaluated in the Schwarzschild term of the GRT acceleration, whereas γ is present in all the terms of (2.10) and in the second term of (2.4). The values obtained in (Combrinck 2011) are somewhat inferior but more rigorous with respect to the initial (Combrinck 2008) tentative results. New results obtained were: values of $\gamma - 1$ are $6.5 \times 10^{-4} \pm 7.4 \times 10^{-4}$ and $9.0 \times 10^{-4} \pm 9.6 \times 10^{-4}$ for LAGEOS 1 and 2 respectively, and values of $\beta - 1$ are $1.2 \times 10^{-3} \pm 1.4 \times 10^{-3}$ and $1.4 \times 10^{-3} \pm 1.5 \times 10^{-3}$ for LAGEOS 1 and 2 respectively. New work is underway, which includes improvement in modelling of the range delay due to the atmosphere, by including an azimuth dependent range delay correction in the SLR analysis software as the atmosphere exhibits nonlinear behaviour (Botai et al. 2010).

2.3.5 Lunar Laser Ranging

Lunar laser ranging (LLR) entails laser ranging to arrays of corner cube reflectors placed on the Moon (see Merkowitz 2010 and references therein for an overview). This high accuracy laser ranging (using equipment similar to SLR, with some system modifications, e.g. using an event timer instead of an interval counter to measure the ToF of the laser pulse) translates to a very accurate orbit determination. The highly accurate orbit can be used for (amongst others) fundamental physics. Placement of the reflectors was done by the Apollo 11, 14 and 15 astronauts, while two French-built reflector arrays were added by the Soviet Luna 17 (the lander carrying robotic rover Lunakhod 1) and Luna 21 missions. Rover Lunakhod 1 was lost in 1971 but relocated using images obtained by the lunar reconnaissance orbiter (LRO). It was consequently ranged to with LLR by Tom Murphy and his team [Apache Point Observatory Lunar Laser-Ranging Operation (APOLLO)], see (Murphy et al. 2007), using the 3.5 m telescope at the Apache Point Observatory in New Mexico. LLR is a sensitive technique to test the equivalence principle (EP).

The EP is the backbone of GRT and involves the equality of gravitational and inertial mass (Newtonian EP). In essence, Einstein's EP (EEP) requires that in local freely falling frames, all physical laws must be independent of the velocity of the frame (i.e. local Lorentz invariance). Furthermore, that two different bodies (such as Earth and the Moon) in a gravitational field (such as that of the Sun) the bodies will experience the same acceleration [weak equivalence principle (WEP)], i.e. EEP requires that the WEP be valid. The strong equivalence principle (SEP) includes the gravitational self-energy of a body in the counting of its total energy content. LLR can also be used to evaluate β, the geodetic precession and $\dot{G}/G$; γ is conveniently used from other high level estimates [such as using the result (Bertotti et al. 2003) of

the radiometric tracking data of the Cassini spacecraft on its approach to Saturn, which gave the best results to date of $\gamma - 1 \, (2.1 \pm 2.3 \times 10^{-5})$].

Similar to SLR, LLR has seen a constant improvement in results due to model and technology improvements. The Earth-Moon-Sun system provides the best laboratory for testing the SEP, with LLR being the only available solar system technique at this time, which may be augmented with interplanetary laser ranging (ILR) in the future. The SEP parameter η is related to the PPN parameters:

$$\eta = 4\beta - \gamma - 3, \tag{2.49}$$

where in GRT $\eta = 0$.

Variation of G in time will be reflected in anomalous evolution of the orbital period of the Moon. If G changes, it will affect the monthly lunar orbit as well as the annual Earth-Moon orbit around the Sun. This is quite evident (Merkowitz 2010) considering Kepler's third law

$$P^2 = \frac{4\pi^2 r^3}{Gm}, \tag{2.50}$$

and by taking the time derivative and re-arranging:

$$\frac{\dot{G}}{G} = 3\frac{\dot{r}}{r} - 2\frac{\dot{P}}{P} - \frac{\dot{m}}{m}. \tag{2.51}$$

After considering factors which make up the non-anomalous orbital evolution (solar perturbation, tidal friction, etc.) (see Williams et al. 1996 for more details) and utilising raging data to the Moon, the anomalous orbital evolution can be estimated and an estimate for $\dot{G}$ derived. In the case of a violation of the EP, a displacement of the lunar orbit along the Earth-Sun line will occur, which will be evidenced in a range signature having a 29.53 day synodic period (not the same as the lunar orbit period of 27 days) (Williams et al. 2009). Some of the LLR tests relating to the fundamental nature of gravity are summarized in Murphy (2009), with short descriptions of the phenomenologies related to SEP, time-rate-of-change of the gravitational constant, gravitomagnetism, inverse square law, and preferred frame effects.

Recent results (Williams et al. 2004) for PPN parameter β are based on $\eta = 4\beta - \gamma - 3$, and are very sensitive to β. Utilising the result of the Cassini spacecraft determination (Bertotti et al. 2003) of $\gamma - 1 \left(2.1 \pm 2.3 \times 10^{-5}\right)$, in combination with $\eta = 4\beta - \gamma - 3 = (4.4 \pm 4.5) \times 10^{-4}$, results in $\beta - 1 = (1.2 \pm 1.1) \times 10^{-4}$. Their test of temporal variation of the gravitational constant delivered the value

$$\frac{\dot{G}}{G} = (4 \pm 9) \times 10^{-13} \text{yr}^{-1}.$$

The LLR network is currently limited to three operational LLR stations, all in the Northern hemisphere. Two stations are located in the USA, the McDonald laser ranging station (MLRS) near Ft. Davis (0.75 m telescope) and the Texas APOLLO

at the Apache Point Observatory in New Mexico (3.5 m telescope). One station (Centre d'Etudes et de Recherche en Géodynamique et Astronomie, CERGA) in France, located at the Observatoire de la Côte d'Azur (OCA) on the Plateau de Calern near Grasse (France), is equipped with a 1.54 m Cassegrain telescope. Even though the LLR network has received a boost through the addition of APOLLO, biases could exist in the ranging solutions as all ranging data are obtained from the Northern hemisphere. In collaboration with OCA and NASA, the Hartebeesthoek Radio Astronomy Observatory (HartRAO) has commenced with a project to develop an LLR system based on an ex-OCA 1 m aperture telescope. This LLR should be operational by 2015 and as it would be dedicated to LLR, should add significantly to the database and strengthen the geometry of the network.

2.3.6 Interplanetary Laser Ranging

Interplanetary laser ranging (ILR) will be able to make a contribution to the dynamics of the solar system and to evaluations of general relativity or alternative theories of gravity by, for instance, ranging to laser transponders placed on suitable planets such as Mars, or ranging to interplanetary probes equipped with laser transponders. In May 2005, timed observations of laser pulses between the Mercury Laser Altimeter (MLA) instrument, which is located onboard the MESSENGER spacecraft, and the Goddard Geophysical Astronomical Observatory (GGAO) (using a 1.2 m telescope) measured the two-way ToF (range) with sub-nanosecond precision (Smith et al. 2006). In addition, a one-way only optical experiment was executed a few months later between GGAO and the Mars Orbiter Laser Altimeter (MOLA) aboard the Mars Global Surveyor (MGS) spacecraft. The distance involved was 81 Gm (0.54 AU). These successful tests demonstrate the possibility of interplanetary communication and precise ranging using modest power (Neumann et al. 2006).

Several possible scenarios utilising ILR have been proposed, including placing an active laser transponder on the Martian moon Phobos with the possibility of millimetre-level ranging resolution (Turyshev et al. 2010). The primary objective of this proposed mission is to measure PPN parameter γ to a level of 2×10^{-7} which would improve today's best result (as determined by radiometric tracking data from the Cassini mission; see Bertotti et al. 2003) by two orders of magnitude. Included in the objectives is a measurement of $\dot{G}$, the time-rate-of-change of the gravitational constant.

It is expected that ILR will make a huge impact on GRT tests, although there will be technical challenges due to the large distances involved. With regard to these future ILR missions, Iorio (2011) has numerically investigated how the ranges between the Earth, the inner planets, as well as Jupiter and Saturn, could be influenced by specified Newtonian and non-Newtonian dynamical effects. This was done by the simultaneous integration of the equations of motion of all the major bodies of the solar system, including Ceres, Pallas, Vesta, Pluto and Eris in the Solar System Barycentric reference frame over a 2 year period, except Mars, Jupiter and Saturn for which a period of 5 years was used.

3 Global Positioning System

The GPS satellites orbit at a height of $\sim 20{,}200$ km. They have an orbital period of about 718 min and a velocity of about 3,874 m/s. This velocity, relative to the geocentre, Earth's rotation and the difference in gravitational potential between observer and the GPS satellite, make it absolutely essential that GRT needs to be considered in timing (frequency) and orbital parameters. The basic theoretical timescale for geodesy and geophysics is Geocentric Coordinate Time, TCG, which is the coordinate time of the GCRS, which has coordinates $(T, \vec{X})$ (Müller et al. 2008; Petit and Luzum 2010).

There are two relativistic effects which affect the clocks of GPS satellites: time dilation and gravitational redshift. The relative motion between the observer (GPS receiver) and the GPS satellite results in special relativistic time dilation, whereas differences in the gravitational potential as experienced by the observer and satellite result in gravitational redshift. As a consequence of these two relativistic effects, so as to align approximately the GPS clocks with terrestrial time (TT), the onboard oscillators require a small frequency (i.e. frequency but not phase aligned, which means a phase delay or advance exists) offset adjustment. Second-order effects resulting from the non-circular orbits have to be corrected in the GPS receiver during processing of observational data by applying a correction of the order of $2(\vec{r} \cdot \dot{\vec{r}})/c^2$, where $\vec{r}$ is the position vector of the satellite (Senior et al. 2008).

3.1 Reference Frame Issues

In the earth-centred inertial (ECI) frame, the special relativistic theory is valid to a high level. The ECI frame is basically a freely falling, local, non-rotating inertial frame with its origin at the centre of the Earth. Although the Earth is accelerating towards the Sun, in this frame, the speed of light can be assumed to be constant. For the purposes of GPS and in general of satellites with clocks on board, it is most convenient (Ashby 2003) to describe their motions in the ECI frame. This approach makes the Sagnac effect irrelevant although the Sagnac effect on Earth-based (moving) receivers must still be taken into account (see Sect. 3.2.3). In the Earth Centred Earth Fixed Frame (ECEF), which is a rotating frame, clock synchronisation is difficult as light travels in a spiral path due to the Sagnac effect. Practically, the ECI is used for the establishment of positions by the GPS; afterwards a rotation to the ECEF is performed.

3.2 Clock and Frequency Effects

Similar to the other space geodetic techniques, the technological basis for GPS is founded on the very stable and accurate atomic clocks used to generate frequencies utilised in the satellite systems, and in the stable quartz oscillators used in GPS

receivers. Higher quality receivers are equipped with better (more stable) oscillators, and for certain demanding applications, for instance the international GNSS service (IGS) receiver (HRAO) at HartRAO, the 5 MHz signal of an external Hydrogen MASER is used as clock reference. A comparison of the modified Allan deviation (MDEV) as calculated from IGS (final product) 30 s satellite clocks active over the period 15 June–5 July 2007 was made by Senior et al. (2008). The MDEV is more suitable when estimating short-term stability and allows distinguishing between white and flicker phase noise (see Riley 2007 for definition and formulation). The comparison includes a listing of the atomic frequency standard (AFS) (caesium or rubidium) and PRN numbers (pseudo-random noise) which is very useful. Included in the comparison were five ground clocks, which were among the highest weighted clocks realizing the IGST (IGS Final) timescale for that period. The HartRAO IGS station (HRAO) using an Oscilloquartz EFOS C passive H-maser as external frequency standard was included, as well as BRUS (Quartzlock CH1-75 active H-maser), BREW (Sigma Tau passive H-maser), STJO (passive H-maser) and NRC1 (Kvarz CH-175 active H-maser).

It is clear from the comparison by Senior et al. (2008) that the GPS satellites have instabilities that are five times greater than the ground clocks. In addition, satellite clock behaviour is dependent on AFS type and constellation block. Block IIA (older block) satellites exhibit 12 h variations (there are also shorter period variations but of lower amplitude, of which the 6 h variation is also significant) up to 8 ns, Block IIR 0.1–0.3 ns and Block IIR-M 0.12 ns. For very accurate applications these variations need to be included in modelling. These clock variations are much smaller than the relativistic effects. The stability of the GPS caesium clocks is such that, after initialisation and an interval of 1 day, the clock would still be correct to ~ 5 parts in 10^{14}, which is about 4 ns (4×10^{-9}s), which is small compared to relativistic effects (Ashby 2003).

3.2.1 Gravitational Redshift

A clock in orbit experiences relativistic shifts which have both constant and time varying components. The constant component can be compensated for by incorporating a fixed offset, which lowers the frequency of the on-board oscillator.

Orbital eccentricity and the quadrupole (including higher order terms) of the Earth's gravity field are primarily responsible for the time varying components (Larson et al. 2007). An arbitrary atomic clock's time τ is associated with TCG in non-rotating GCRS coordinates by (Müller et al. 2008) so that

$$\frac{d\tau}{dTCG} = 1 - \frac{1}{c^2}\left(U + \frac{1}{2}\vec{v}^2\right) + \mathcal{O}(c^{-4}), \qquad (2.52)$$

where the speed of light in vacuum is denoted by c, $\vec{v}$ is the GCRS speed of the satellite and the GCRS gravitational potential at the clock is U. Several gravitational components are contained within U. Earth's tidal potential U_E is the main

constituent, although also included are the tidal potentials of the Sun, Moon and planets U_{tidal} and U_{iner}, an inertial component. A more detailed description of these components can be found in Müller et al. (2008).

As an example (Müller et al. 2008), if two clocks are located on an equipotential surface, the rates of the clocks will be the same. If however, one clock is moved to a height of 1 km, their rates would differ by about 10^{-13}. The gravitational redshift can then be written (Larson et al. 2007) in terms of the Newtonian gravitational potential $\Phi(\vec{r})$ at the point $\vec{r}$ of the GPS satellite in orbit as

$$\frac{\Delta f}{f} = \frac{\Phi(\vec{r}) - \Phi_0}{c^2}. \tag{2.53}$$

In (2.53) Φ_0 is the gravity potential (including the centrifugal potential resulting from the rotation of Earth) at the reference clock located on Earth's geoid. The International Astronomical Union (IAU) has defined (IAU Resolutions 2000, Resolution B1.9) the relation Φ_0/c^2 by setting the relation between TCG and TT to have a rate of $-6.969\,290\,134 \times 10^{-10}$ (Kaplan 2005; Burša et al. 2007). Considering the reference clock located on the geoid, the potential at Φ_0 is approximately (cf. Cazenave 1995; Kouba 2004; Ashby and Nelson 2009)

$$\Phi_0 = -\frac{GM}{r_\theta}\left(1 - \frac{J_2 \cdot r_{eq}^2}{r_\theta^2} \cdot \frac{1}{2}\left(3\sin^2\theta - 1\right)\right) - \frac{1}{2}\left(\omega r_\theta \cos\theta\right)^2, \tag{2.54}$$

where the first term makes up the static component and the second is the centrifugal component. In (2.54), θ is measured north or south from the equator, r_θ is the radius of Earth at the specified latitude and $r_{eq} = 6.378\,137 \times 10^6\ m$ is the equatorial radius of Earth. The angular velocity of Earth's rotation is $\omega = 7.291\,151\,467 \times 10^{-5}$ rad/s. Earth's quadrupole moment (coefficient) $J_2 = 1.08268 \times 10^{-3}$ accounts for the oblateness of the Earth. Considering a reference clock on the equator (clocks on the equator essentially run at the same rate as clocks that are not on the equator due to higher gravitational redshift at higher latitudes, more time dilation on the equator and a correction due to the quadrupole; these effects compensate to a high level; see Ashby 2006), one can rewrite (2.54) where $\theta = 0$, as

$$\Phi_0 = -\frac{GM}{r_{eq}}\left(1 + \frac{J_2}{2}\right) - \frac{1}{2}\left(\omega r_{eq}\right)^2. \tag{2.55}$$

Earth's quadrupole's effect on the potential at the GPS satellite is approximately one part in 10^{14} (Ashby 2005), so in the case of the potential at the satellite, the contribution of the quadrupole can be ignored in most cases (GPS orbits are high enough to be nearly Keplerian); there is also no centrifugal component so that the gravitational potential at the GPS satellite is to a good approximation

$$\Phi_{GPS} = \frac{-GM}{|\vec{r}|}. \tag{2.56}$$

The total gravitational frequency shift of the clock onboard the GPS satellite can then be calculated using (2.53) as (Ashby 2003, 2006; Larson et al. 2007)

$$
\begin{aligned}
\frac{\Delta f}{f} &= \frac{\Phi_{GPS} - \Phi_0}{c^2} \\
&= -\frac{GM}{c^2|\vec{r}|} - \left(-\frac{GM}{r_e c^2}\left(1 + \frac{J_2}{2}\right) \right) \\
&\approx 5.288 \times 10^{-10} \approx 45.688\,\mu\text{s.d}^{-1}.
\end{aligned}
\tag{2.57}
$$

Ignoring this increase of the satellite clock frequency will lead to a timing error and consequent navigational (one way range ρ) error (per day) of

$$
\begin{aligned}
\rho_{error} &= c \times \frac{\Delta f}{f} \\
&= 299792458.0 \times 4.5688 \times 10^{-5} \\
&\approx 13.697 \text{ km.}
\end{aligned}
\tag{2.58}
$$

3.2.2 Special Relativity: Second Order Doppler Effect

As a consequence of the high speed (~ 3874 m/s) of GPS satellites, the special relativity theory of Einstein needs to be applied. The time dilation effect causes the GPS satellite to appear to run slow by about $7\,\mu\text{s.d}^{-1}$. Using the mathematical formalism of general relativity, a specified reference system is fixed by the specific form of the metric tensor $g_{\alpha\beta}(t, x^i)$. The metric tensor allows (Soffel et al. 2003) calculation of the 4-distance ds between any two events x^α and $x^\alpha + dx^\alpha$ following the rule

$$
\begin{aligned}
ds^2 &= g_{\alpha\beta}(t, x^i)dx^\alpha dx^\beta \\
&\equiv g_{00}c^2 dt^2 + 2g_{0i}c\,dt\,dx^i + g_{ij}dx^i dx^j.
\end{aligned}
\tag{2.59}
$$

In (2.59) Einstein's summation convention is implied. Four coordinates $x^\alpha = (x^0, x^i) = (x^0, x^1, x^2, x^3)$ describe the four-dimensional space–time reference system. Greek indices adopt the values 0, 1, 2 and 3; Latin indices adopt the values 1, 2 and 3. Indices 1, 2 and 3 refer to the three spatial coordinates and index 0 refers to the time variable. For dimensional reasons, $x^0 = ct$ is normally used. Here the speed of light is denoted by c and t is a time variable. Translational and rotational equations of motion of bodies can be derived using the metric, allowing one to describe the propagation of light and to model the process of observation. For instance, one can model the relationship between the observed (proper) time τ of an observer and the coordinate time t. Proper time is the time actually read at the clock. Coordinate time is the time specified by the time coordinate x^0. In terms of a specific model, these components can be combined into a relativistic model. Refer to Soffel et al. (2003) for more details.

Following Nelson and Ely (2006), we derive the relativistic effect (one of the many formulations of it, cf. Larson et al. 2007) on a GPS satellite's clock time in general, including the relativistic time dilation, and conclude with approximate formulations (typically used) of the corrections to be applied to the satellite clocks.

In an ECI frame the components of the metric tensor can be written as (cf. Soffel et al. 2003, discussion of the metric tensor for space–time coordinate systems $(t, \vec{x})$, which are centred at the barycentre of an ensemble of masses)

$$
\begin{aligned}
-g_{00} &\approx 1 - 2U/c^2 \\
g_{0j} &= 0 \\
g_{ij} &\approx \delta_{ij},
\end{aligned}
\tag{2.60}
$$

as an approximation in the analysis of clock transport. In (2.60) the Newtonian gravitational potential is denoted by U and δ_{ij} is the Kronecker delta. For a clock on board the GPS satellite, the elapsed coordinate time can be expressed in terms of the proper time by the integral

$$
\Delta t = \int_{\tau_0}^{\tau} \left(1 + \frac{1}{c^2} U + \frac{1}{2}\frac{1}{c^2} v^2 \right) d\tau.
\tag{2.61}
$$

In (2.61) under the integral, proper time, gravitational redshift and time dilation are the first, second and third term respectively. The magnitude of the time dilation can be expressed as (Zhang et al. 2006)

$$
\Delta f_r \equiv f_s \left(1 - \frac{\vec{r}_T}{c} \right) \left(\frac{v^2}{2c^2} \right) = \frac{f_s v^2}{2c^2} - \frac{f_s \vec{r}_T v^2}{2c^3} \approx \frac{f_s}{2} \frac{v^2}{c^2}.
\tag{2.62}
$$

In (2.62) $\vec{r}_T$ is the GPS satellite transversal velocity, v is its tangential velocity, f_r is the frequency received at the receiver and f_s is the original frequency of the transmitter. The GPS L1 and L2 frequencies are in the Gigahertz range, so the frequencies are high enough (for L1 $\lambda = 1.57542$ GHz, for L2 $\lambda = 1.22760$ GHz) to make the Doppler effect considerable, as

$$
D \equiv f_r - f_s = \frac{\vec{r}_T}{c} f_s = \frac{1}{\lambda} \vec{r}_T
\tag{2.63}
$$

Considering that $f_r > 0.1$ Hz, which translates to more than 2 cm/s error in the range rate, the second-order Doppler effect cannot be neglected for geodetic applications. The order of magnitude of the time dilation effect is (Ashby 2006)

$$
-\frac{1}{2}\frac{v^2}{c^2} \approx -8.35 \times 10^{-11}.
\tag{2.64}
$$

As the reference clock (in the receiver) is also moving, although at a lower speed (~ 465 m/s) relative to the GPS satellite, the fractional frequency difference

due to time dilation between a GPS satellite clock and a reference clock on the equator can be obtained by calculating the difference,

$$\frac{\Delta f}{f} = -\frac{1}{2}\frac{v^2}{c^2} - \left(-\frac{1}{2}\frac{(\omega r_e)^2}{c^2}\right) = -8.228 \times 10^{-11}. \tag{2.65}$$

In (2.65) ω is the angular velocity of Earth and r_e is Earth's equatorial radius. This fractional frequency shift, if not considered, would lead to a navigational error of 2.13 km/day (Ashby 2006). The negative value indicates that the satellite clock runs slow relative to the reference clock on the equator.

Continuing with the reasoning of Nelson and Ely (2006), a new coordinate time can be defined (in the ECEF frame) by applying a change of scale:

$$\Delta t' = \left(1 - \frac{1}{c^2} W_0\right)\Delta t = \int_{\tau_0}^{\tau} \left\{1 + \frac{1}{c^2}(U - W_0) + \frac{1}{2}\frac{1}{c^2}v^2\right\}d\tau. \tag{2.66}$$

In (2.66) W_0 equals Φ_0 as defined in (2.54) and (2.55) and U equals $\Phi(\vec{r})$ as defined in (2.53) and (2.56) where for our purposes $\Phi(\vec{r}) = \Phi_{\text{GPS}}$. Coordinate time $\Delta t'$ represents proper time of the reference clock at rest on the geoid and is therefore the coordinate clock. The elapsed coordinate time for the GPS satellite clock after integration is (Nelson and Ely 2006)

$$\Delta t' = \left(1 + \frac{3}{2}\frac{1}{c^2}\frac{GM}{a} - \frac{1}{c^2} W_0\right)\Delta\tau + \frac{2}{c^2}\sqrt{GMa}\, e \sin E. \tag{2.67}$$

In (2.67) a, e and E are the semi-major axis, eccentricity and eccentric anomaly of the GPS satellite orbit respectively. A constant rate offset is contained within the first term; this offset is between the satellite clock and a reference clock on the geoid whereas the second term results from orbital eccentricity and leads to a small relativistic periodic correction (amplitude of ~ 30 ns), which has to be corrected by the GPS receiver software. According to Ashby (2003) the clocks in the GLONASS satellite are adjusted before broadcast. It would seem that the GPS system carries some historical baggage, as the decision to have the user make the orbital eccentricity correction was due to the weak computing power available in the early GPS satellite vehicles.

In (2.67) there are two constant rate corrections in the first term. Extending (Ashby 2003) and adding the time dilation contribution as described by (2.65) so that the formulation equals that of Ashby (2006) one has three constant rate terms

$$\frac{3}{2}\frac{1}{c^2}\frac{GM}{a} - \frac{\Phi_0}{c^2} - \frac{1}{2}\frac{(\omega r_e)^2}{c^2} = -4.4647 \times 10^{-10}. \tag{2.68}$$

This constant rate in (2.68) can be explained (Ashby 2006) by reviewing the total contribution of the fractional frequency shift, which is obtained by addition. If one combines (2.57) with (2.65),

$$\left(\frac{\Delta f}{f}\right)_{\text{net}} = -\frac{GM}{c^2|\vec{r}|} - \left(-\frac{GM}{r_e c^2}\left(1+\frac{J_2}{2}\right)\right) + \left(-\frac{1}{2}\frac{v^2}{c^2} - \left(-\frac{1}{2}\frac{(\omega r_e)^2}{c^2}\right)\right), \quad (2.69)$$

considering that the total energy per unit mass of the satellite is

$$\frac{1}{2}v^2 - \frac{GM}{r} = -\frac{GM}{2a} \quad (2.70)$$

In (2.70) $a = 26.562 \times 10^3$ km is the semi-major axis of a GPS satellite orbit. The velocity term in (2.69) can be removed by keeping r and a, which (Ashby 2006) leads to the equation

$$\frac{\Delta f}{f} = -\frac{2GM}{c^2}\left(\frac{1}{r} - \frac{1}{a}\right) - \frac{3GM}{2c^2 a} + \frac{GM}{c^2 r_e}\left(1+\frac{J_2}{2}\right) + \frac{1}{2}\frac{(\omega r_e)^2}{c^2}. \quad (2.71)$$

In (2.71) the first term will disappear when the orbit has zero eccentricity. This leaves us with the constant part as described by (2.68).

The GPS satellite clocks are adjusted for the three constant rate corrections before launching them into orbit, the negative sign of (2.68) implying that the satellite clock has a higher frequency in orbit than on the ground (read geoid, where the clock frequency should be 10.23 MHz) and its proper frequency should therefore be reduced to

$$\left(1 - 4.4647 \times 10^{-10}\right) \times 10.23\,\text{MHz} = 10.229\,999\,995\,43\ \text{MHz}. \quad (2.72)$$

The second term in (2.67) (to be corrected by the user's software) may be written as

$$\Delta t_{\text{rel}} = \frac{2}{c^2}\sqrt{GMa}\,e\,\sin E \quad (2.73)$$

and (2.73) can be written as

$$\Delta t_{\text{rel}} = \frac{2\vec{r}\cdot\dot{\vec{r}}}{c^2} \quad (2.74)$$

The dot product of the position vector $\vec{r}$ and velocity vector $\dot{\vec{r}}$ in (2.74) is a scalar; one can therefore use it in the ECI or in the ECEF coordinate system. Equations (2.73) and (2.74) are formulations (which include only the main monopole contribution of Earth's gravity field) often used in precise geodetic applications and are accurate to a sufficient level for most GPS applications, but are inadequate when evaluating lower orbits such as GRACE (Larson et al. 2007). More exact formulations of (2.73) and (2.74) can be found in Kouba (2004) and Larson et al. (2007).

3.2.3 Sagnac Effect

In addition to the gravitational red (blue)-shift and time-dilation effects, a further effect involves the second postulate of special relativity (the constancy of the speed of light), the fundamental principle on which the Global Positioning System is based. As already mentioned, it is convenient to synchronise clocks in an ECI frame as light does not travel in a straight line in a rotating frame. This excludes an ECEF frame from being used to synchronise clocks, due to the Sagnac effect. A stationary GPS receiver located on the equator will have a velocity of ~465 m/s through the ECI frame as the Earth rotates. The corresponding Sagnac correction can be as large as 133 ns (equal to 86 ms signal propagation). This correction is also applied in the receiver. Allowing for the Sagnac effect in the ECEF is equivalent to correcting for the receiver's motion in the ECI frame (Ashby 2002).

Following Ashby (2006), to determine position using the GPS, three satellites are required for position and four are required to determine position and time. Clocks onboard the satellites are synchronised in the ECI frame. A user GPS_{user} will receive time signals at a specific time and position, whereas the GPS satellites will transmit signal messages containing the time and position of the transmission events, so that

$$
\begin{aligned}
GPS_{user} &= \{t_u, \vec{r}_u\} \\
GPS_{sat} &= \{t_j, \vec{r}_j\} \quad j = 1\ldots n,
\end{aligned}
\tag{2.75}
$$

where j is the number of the GPS satellite from which data are being received and n is the total number in view. The constancy of the speed of light is then represented by

$$
c(t - t_j) = |\vec{r} - \vec{r}_j|; \quad j = 1\ldots n.
\tag{2.76}
$$

The nonlinear system (2.76) needs to be solved to provide the user's position; this can be done by linearising the equations and initialising an iterative algorithm with an a priori position. Due to the motion of the GPS receiver, the navigation equations in (2.76) are not valid in the ECEF frame. Most of the time, of course, users would want their positions in the ECEF, not in an ECI frame. In the ECEF, the rotation of Earth will move the GPS receiver while the GPS signal is propagating to Earth, so (2.76) needs to be altered to account for this as

$$
t = t_j + \frac{|\vec{r}(t) - \vec{r}_j|}{c} = \frac{|\vec{r}(t_j) + \vec{v} \times (t - t_j) - \vec{r}_j|}{c}.
\tag{2.77}
$$

In (2.77) the receiver position at time t is denoted by $\vec{r}(t)$ and $\vec{v}$ is the velocity of the receiver at the time of the GPS satellite transmission. The velocity of the receiver is far less than that of c, and therefore the equations can be solved through an iteration algorithm. An iteration algorithm was also required to find the two-range as determined through SLR as discussed in Sect. 2.2.1. The range from GPS satellite to receiver can be defined as

$$\vec{R} = \vec{r}(t_j) - \vec{r}_j \qquad (2.78)$$

and excluding the velocity term we get the time of arrival of the signal if it were in the ECI frame:

$$t = t_j + \frac{\left|\vec{r}(t_j) - \vec{r}_j\right|}{c} = t_j + \frac{R}{c}. \qquad (2.79)$$

If t is substituted back into (2.77) then one can find (Ashby 2006)

$$t = t_j + \frac{\sqrt{R^2 + 2\vec{R} \cdot \vec{v}(t - t_j)}}{c} \approx \frac{R}{c} + \frac{\vec{R} \cdot \vec{v}}{c^2}. \qquad (2.80)$$

In the case where the receiver's velocity is only a result of the rotation of Earth, then

$$\vec{v} = \vec{\omega} \times \vec{r}(t_j) \qquad (2.81)$$

and one can rewrite the Sagnac correction term as

$$\Delta t_{\text{Sagnac}} = \frac{\vec{R} \cdot \vec{v}}{c^2} = \frac{2\vec{\omega} \cdot \vec{A}}{c^2} \qquad (2.82)$$

with the vector area $\vec{A}$ being given by

$$\vec{A} = \frac{1}{2}\vec{r}(t_j) \times \vec{R}. \qquad (2.83)$$

In (2.81) and (2.82) $\vec{\omega} = (0, 0, \omega)$. The dot product in (2.82) projects area $\vec{A}$ (the Sagnac correction is proportional to this area) onto a plane that is parallel to the equatorial plane. Area $\vec{A}$ is created by the sweeping vector from the rotation axis to tip of the signal pulse as it propagates from transmitter to receiver (Ashby 2004). Area $\vec{A}$ is therefore swept out by the electromagnetic pulse as it propagates from the GPS satellite transmitter to the receiver.

3.3 General Relativistic Accelerations

The relativistic accelerations in the weak-field and slow motion approximation as described by the standard IERS formulation (2.10) for the Schwarzschild field, frame dragging and de Sitter precession are additional relativistic effects, which should be taken into account during POD. Table 2.1 lists the magnitude of these effects when considering GPS satellites.

3.4 Spatial Curvature Effect on Geodetic Distance

The proper distance between a receiver on the surface of the Earth at radius r_1 and a GPS satellite at radius r_2 is approximately (Ashby 2003)

$$\int_{r_1}^{r_2} \left[1 + \frac{GM}{c^2 r} \right] dr = r_2 - r_1 + \frac{GM}{c^2} \ln\left(\frac{r_2}{r_1}\right). \qquad (2.84)$$

Using (2.84) and, in addition, calculating the coordinate distance, the difference between proper and coordinate distance is about 6.3 mm ((2.4) as applied to SLR).

4 Very Long Baseline Interferometry

Observations of compact extragalactic radio sources using the technique of VLBI are very well suited to the study of Earth orientation in space, as these sources serve as an excellent approximation to an inertial frame. The VLBI technique is unique in that it provides Earth orientation measurements of high accuracy in an inertial frame of reference (Sovers et al. 1998). Similar to the other space geodetic techniques, the reduction of VLBI data requires consideration of a large range of effects, which include the effects of the Earth's internal structure on its dynamics, the VLBI site velocity as caused by tectonic plate motion, terrestrial tidal effects, and quantification of tropospheric and ionospheric parameters. In addition, consideration must be given to special relativity in the interpretation of the radio signals travelling from the distant sources, as well as to general relativistic retardation. For a thorough introduction to VLBI the reader should refer to the chapter by Harald Schuh and Johannes Böhm in this volume, in which is included a discussion of the VLBI GRT model for propagation. I will attempt to provide additional information which could be read in the context of and as ancillary material to the Schuh and Böhm chapter without unnecessary repetition.

4.1 Gravitational Delay

According to GRT, an electromagnetic signal will experience retardation in terms of its travel time when propagating in a gravitational potential relative to its propagation in gravity field-free space. This has implications for VLBI, as the value determined for the difference in arrival time at the VLBI stations in question must be corrected for gravitational effects. Furthermore, considering the implications of GRT, one must take into account both a time delay (Shapiro 1964) and a bending delay (deviation from a straight-line path) (Shapiro 1967). The current general relativistic VLBI model for propagation used by international VLBI

service (IVS) analysis centres is the IERS (Petit and Luzum 2010) recommended "consensus model" (Eubanks 1991) which provides an accuracy below 1 ps as described inChap.11of the IERS Conventions. According to Petit (2009) there are no changes expected in the short term, although a review is possible in the light of future VLBI accuracy improvements. This is true specifically with regard to VLBI2010, which will require that the consensus model be re-evaluated to ensure that it includes all terms down to the order of 0.3 ps (Heinkelmann and Schuh 2009). Objectives of VLBI2010 include 1 mm position accuracy over a 24 h observing session (on global baselines), 0.1 mm/year station velocity accuracy, continuous observations, and delivery of initial results within 24 h after taking data (MacMillan et al. 2011)

4.2 General Relativistic Tests Using VLBI

VLBI currently achieves very high accuracies, better than 0.1 mas. These high accuracies make VLBI an excellent tool for GRT tests and evaluation and therefore the geodetic VLBI technique has often been used to evaluate the space curvature parameter γ introduced in (2.4). Tests of special and general relativity were quickly launched after Einstein's publications. Acceptance of relativity was not instantaneous and general acceptance was fraught with misunderstanding, political viewpoints, self-serving attitudes and the typical slow acceptance of a new scientific doctrine. A very good review of the early tests and human drama involving astronomers of the early twentieth century is given in Crelinsten (2006). These tests involved gravitational redshift and light bending (primarily light deflection at the Sun's limb during eclipses). Currently one of the most accurate methods to evaluate γ is by utilising VLBI.

The space–time geometry around the Sun can be described by a static and spherically symmetric metric (Schwarzschild 1916). However, Eddington (1923) provided an isotropic formulation of Schwarzschild's original anisotropic version of the metric (2.21) (where, as noted by Eddington, in the original coordinates, the speed of light is not the same for transverse and radial directions), which can be written as

$$ds^2 = -\left(1 - 2\frac{GM}{c^2 r} + 2\left(\frac{GM}{c^2 r}\right)^2\right)(cdt)^2 + \left(1 + 2\frac{GM}{c^2 r}\right)\left[dx^2 + dy^2 + dz^2\right].$$

(2.85)

Here the gravitational constant is G, the speed of light is given by c and M is the mass of the star (Sun). The PPN parameters γ and β are the most physically significant of the ten parameters in the PPN formalism and this is demonstrated by their placement (Margot and Giorgini 2009) in (2.85):

$$ds^2 = -\left(1 - 2\frac{GM}{c^2 r} + 2\beta\left(\frac{GM}{c^2 r}\right)^2\right)(cdt)^2 + \left(1 + 2\gamma\frac{GM}{c^2 r}\right)\left[dx^2 + dy^2 + dz^2\right].$$

$$(2.86)$$

In the first term on the right-hand side of (2.86) β describes the degree of nonlinearity in the superposition law for gravity, while the second term (spatial part) contains PPN γ, which describes how much curvature is produced by unit rest mass, and can be tested by deflection of light, bending of radio waves and Shapiro delay experiments. In GRT both parameters γ and β are equal to unity, whereas the other eight PPN parameters are zero (Will and Nordtvedt 1972).

4.2.1 Evaluation of PPN Parameter γ

The classical test by Eddington on the deflection of light by the Sun (Dyson et al. 1920) and the delay of an electromagnetic signal as it propagates near the Sun (Shapiro et al. 1968) essentially measure the propagation of photons in curved space near the Sun; these measurements depend on the PPN parameter γ. The amount of space curvature per unit mass is related to γ through the proportional relationship

$$\delta\theta \propto 1/2(1 + \gamma).$$

$$(2.87)$$

Following Will (2006), an electromagnetic signal (ray of light or radio signal from VLBI source) passing close to the Sun at distance d will be deflected by an angle,

$$\delta\theta = \frac{1}{2}(1 + \gamma)(4m_\odot/d)[(1 + \cos\Phi)/2],$$

$$(2.88)$$

where the mass of the Sun is denoted by $m_\odot$ and Φ is the angle formed between the direction of the incoming electromagnetic signal and the line between Earth and the Sun. The relative angular separation may be changed when the line-of-sight of one of the sources moves close to the Sun. This angular separation is given by

$$\delta\theta = \frac{1}{2}(1 + \gamma)\left[-\frac{4m_\odot}{d}\cos\chi + \frac{4m_\odot}{d_r}\left(\frac{1 + \cos\Phi_r}{2}\right)\right].$$

$$(2.89)$$

In (2.89) the points of closest approach to the Sun in terms of distance are given by d and d_r for the source and reference rays, respectively. The angle created by the Sun-source and Sun-reference directions, projected against the plane of the sky, is given by χ and Φ_r denotes the angle between the reference source and the Sun. More details can be obtained from Will (2006). This short introduction describes the basics for the determination of the varying relative angular separation as would be determined using VLBI, when the line-of-sight of a radio source is close to the Sun,

$$d \sim R_\odot, \, d_r \gg d$$

and χ is varying with time. Of course the Sun could be replaced by a large planet such as Jupiter (see for instance Schuh et al. 1988; Fomalont and Kopeikin 2003) and the radio source could be a transmitter on board an interplanetary probe. The literature abounds with comparisons between the results of different (e.g. radar determined) techniques but here we focus on VLBI (cf. Pitjeva 2005; Turyshev 2009).

Constant instrumental and data analysis upgrades throughout the development of the VLBI technique have delivered a continuous increase in the accuracy of the evaluations of PPN parameter γ. This continuous improvement is illustrated in Fig. 2.2, which is based on the table of γ estimates spanning the period 1972–2009 as provided by Heinkelmann and Schuh (2009). Figure 2.2 contains the standard error of the various γ estimates, reflecting the accuracy of the parameter evaluation. An exponential fit constrained to the first and last estimate provides a value of $\pm\, 2.5 \times 10^{-5}$, when using the fitted function to predict towards 2020. If this predicted accuracy level is achieved by VLBI, perhaps supported by the developments around VLBI2010 in the GGOS framework, it would be comparable to the accuracy (currently the best) of the estimate of γ ($\pm 2.3 \times 10^{-5}$) achieved during the microwave tracking of the Cassini spacecraft on its approach to Saturn (Bertotti et al. 2003). Evaluations represented in Fig. 2.2 are contained in Table 2.2.

The gravitational signal retardation (Shapiro effect) is described by

$$\tau_{\text{grav}} = (1 + \gamma) \cdot \frac{GM}{c^3} \cdot \ln \left[\frac{\left| \vec{X}_1 \right| + \vec{X}_1 \cdot \vec{k}}{\left| \vec{X}_2 \right| + \vec{X}_2 \cdot \vec{k}} \right], \tag{2.90}$$

where $\vec{X}_i$ is the position vector of the individual VLBI antennas relative to the centre of the gravitating body and the unit vector towards the radio source as viewed from the Earth-bound baseline is denoted by $\vec{k}$. Following Heinkelmann and Schuh (2009), the partial derivative of the delay relative to γ can be written as

$$\frac{\partial \tau}{\partial \gamma} = \frac{GM}{c^3} \cdot \ln \left[\frac{\left| \vec{X}_1 \right| + \vec{X}_1 \cdot \vec{k}}{\left| \vec{X}_2 \right| + \vec{X}_2 \cdot \vec{k}} \right], \tag{2.91}$$

which will be required for the estimation of γ utilising the Shapiro delay in a least-squares process. A typical value for the Shapiro delay due to the gravitational field of the Earth (see Table 2.1) for a baseline of 6000 km, is about 21 ps (Klioner 1991). The Shapiro time delay that results from the Sun for the same baseline length can vary from 17×10^4 ps for an electromagnetic ray grazing the Sun's limb to about 17 ps when the rays are incident at about $90°$ from the Sun. Models for the gravitational delay are continuously improved (cf. Klioner and Kopeikin 1992; Kopeikin and Schäfer 1999). An additional delay, which is caused by the effect due to the finite speed of the propagation of gravity, may have to be included (Kopeikin 2001). This delay could be at the level of several ps; however, recent refinements and the formulation of higher level models (utilising these refinements) have not completely been incorporated into the standard IERS formulation.
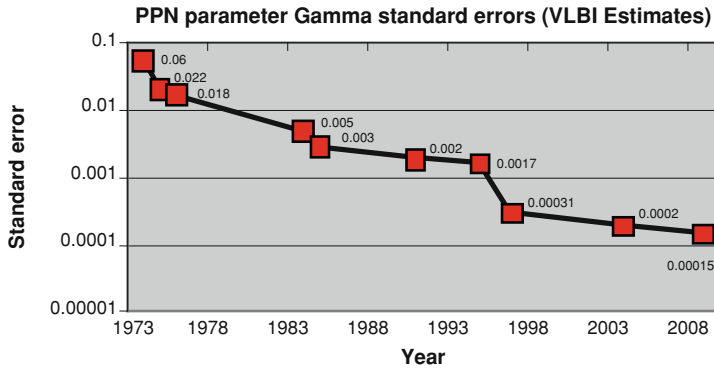
PPN parameter Gamma standard errors (VLBI Estimates)

Fig. 2.2 Standard errors associated with geodetic VLBI evaluations of PPN parameter γ. Continuous improvement is due to instrumentation, software and model development as well as longer time series of data

Table 2.2 Standard errors associated with geodetic VLBI evaluations of PPN parameter γ

Authors	Standard error
Counselman et al. (1974)	± 0.06
Fomalont and Sramek (1975)	± 0.022
Fomalont and Sramek (1976)	± 0.018
Robertson and Carter (1984)	± 0.005
Carter et al. (1985)	± 0.003
Robertson et al. (1991)	± 0.002
Lebach et al. (1995)	± 0.0017
Eubanks et al. (1997)	± 0.00031
Shapiro et al. (2004)	± 0.00021
Lambert and Le Poncin-Lafitte (2009)	± 0.000152

5   Concluding Remarks

It is very rewarding to see, throughout the development of the Space Geodetic techniques, how theory, experiment, human innovation and the constant drive towards better science and higher accuracies have meshed to form global networks of instruments and people. Applications of space geodesy extend from outer space to the core of the Earth; they utilise and are capable of testing and evaluating GRT.

Future improvements, within the framework of GGOS, will provide improved accuracies and a better understanding of the space and world in which we live. General relativity will continue to be tested by scientific experiments in which space geodesy has its own specific role to play, providing certainty on the levels to which GRT can reliably be used; eventually, however, experiments will lead to a post-GRT theory. Exciting scientific projects based on space geodesy are on the horizon which will play a role in the evaluation of GRT. These include

densification and upgrade of the existing International Laser Ranging Service Network (ILRS) SLR network, the development of VLBI2010, ILR and expansion of the LLR network to the southern hemisphere with the development of an LLR system at HartRAO, South Africa.

References

Ashby N, Shahid-Saless B (1990) Geodetic precession or dragging of inertial frames? Phys Rev D 42:1118–1122

Ashby N (2002) Relativity and the global positioning system. Phys Today 55(5):41–47

Ashby N (2003) Relativity in the global positioning system. Living Rev Relativ, vol 6, p 1 [http://www.livingreviews.org/Articles/Volume6/2003-1ashby, online article: cited on 7 July 2010]

Ashby N (2004) The sagnac effect in the global positioning system. In: Rizzi G, Ruggiero ML (eds) Relativity in rotating frames, Kluwer Academic Publishers, Dordrecht, The Netherlands, pp 11–28

Ashby N (2005) Relativity in the global positioning system. In: Ashtekar A (ed) 100 years of relativity space-tine structure: Einstein and beyond. World Scientific Publishing Co, Singapore, pp 257–289

Ashby N (2006) Relativistic effects in the global positioning system. http://www.aapt.org/doorway/tgru/articles/Ashbyarticle.pdf, online article: cited on 1 May 2011

Ashby N, Nelson RA (2009) The global positioning system, relativity and extraterrestrial navigation, in relativity. In: lioner SA, Seidelmann PK, Soffel MH (eds) Fundamental astronomy: dynamics, reference frames, and data analysis proceedings IAU symposium no. 261, Cambridge University Press, pp 22–30

Bertotti B, Iess L, Tortora P (2003) A test of general relativity using radio links with the cassini spacecraft. Nature 425:374–376

Beutler G, Drewes H, Verdun A (2005a) The integrated global geodetic observing system (IGGOS) viewed from the perspective of history. J Geodyn 40(4–5):414–431

Beutler G, Mervart L, Verdun A (2005b) Methods of celestial mechanics: application to planetary system, geodynamics and satellite geodesy, vol II. Springer, Germany

Botai OJ, Combrinck L, Sivakumar V, Schuh H, Böhm J (2010) Extracting independent local oscillatory geophysical signals by geodetic tropospheric delay. In: IVS 2010 general meeting proceedings, pp 345–354. http://ivscc.gsfc.nasa.gov/publications/gm2010/botai.pdf

Burša M, Kenyon S, Kouba J, Šíma Z, Vatrt V, Vítek V, Vojtíšková M (2007) The geopotential value w_0 for specifying the relativistic atomic time scale and a global vertical reference system. J Geod 81:103–110

Carter WE, Robertson DS, MacKay JR (1985) Geodetic radio interferometric surveying: applications and results. J Geophys Res 90(B6):4577–4587

Cazenave A (1995) Geoid, topography and distribution of landforms, in global earth physics; a handbook of physical constants, American Geophysical Union

Ciufolini I (1986) Measurement of the lense-thirring drag on high-altitude laser- ranged artificial satellites. Phys Rev Lett 56:278–281

Ciufolini I, Wheeler JA (1995) Gravitation and inertia. Princeton University Press, Princeton

Ciufolini I, Lucchesi DM, Vespe F, Mandiello A (1996) Measurement of dragging of inertial frames and gravitomagnetic field using laser-ranged satellites, Il. Nuovo Cimento A 109:575–590

Ciufolini I, Pavlis E, Chieppa F, Fernandes-Vieira E, Pérez-Mercader J (1998) Test of general relativity and measurement of the lense-thirring effect with two earth satellites. Science 279:2100–2103

Ciufolini I, Pavlis EC (2004) A confirmation of the general relativistic prediction of the lense–thirring effect. Nature 431:958–960

Ciufolini I, Pavlis EC, Peron R (2006) Determination of frame-dragging using earth gravity models from CHAMP and GRACE. New Astron 11:527–550

Ciufolini I (2007) Gravitomagnetism, frame-dragging and lunar laser ranging, arXiv: 0704.3338v2 [gr-qc], 10 May 2007

Combrinck L (2008) Evaluation of PPN parameter gamma as a test of general relativity using SLR data. In: 16th international laser ranging workshop, (Poznan (PL) 13–17 Oct 2008), available at http://cddis.gsfc.nasa.gov/lw16/docs/papers/sci_6_Combrinck_p.pdf

Combrinck L (2010) Satellite laser ranging. In: Xu Guochang (ed) Sciences of Geodesy I, advances and future directions. Springer, Germany, pp 301–336

Combrinck L (2011) Testing general relativity theory through the estimation of PPN parameters γ and β using satellite laser ranging data. S Afr J Geol 114(3–4):549–560

Counselman CC, Kent SM, Knight CA, Shapiro II, Clark TA, Hinteregger HF, Rogers AEE, Whitney AR (1974) Solar gravitational deflection of radio waves measured by very-long-baseline interferometry. Phys Rev Lett 33(27):1621–1623

Crelinsten J (2006) Einstein's jury: the race to test relativity. Princeton University Press, Princeton

Cugusi L, Proverbio E (1977) Relativistic effects on the motion of the earth's satellites. In: Paper presented at the international symposium on satellite geodesy in Budapest from 28 June to 1 July 1977, J Geodesy, vol 51, pp 249–252

Cugusi L, Proverbio E (1978) Relativistic effects on the motion of earth's artificial satellites. Astron Astrophys 69:321–325

Damour T, Soffel M, Xu C (1994) General-relativistic celestial mechanics IV. Theory of satellite motion. Phys. Rev. D 49:618–635

de Sitter W (1916) On Einstein's theory of gravitation and its astronomical consequences. Mon Not Roy Astron Soc 77:155184

Drewes H (2007) science rationale of the global geodetic observing system (GGOS), in dynamic planet, monitoring and understanding a dynamic planet with geodetic and oceanographic tools. In: Tregoning P, Rizos C (eds) Planet earth. IAG Symposia, vol 130. Springer, pp 703–710

Dyson FW, Eddington AS, Davidson C (1920) A determination of the deflection of light by the sun's gravitational field, from observations made at the total eclipse of 29 May 1919. Phil Trans R Soc Lond A 220:291–333

Eddington AS (1923) The mathematical theory of relativity. Cambridge University Press, UK

Einstein A (1920) Relativity: the special and general theory. Henry Holt and Company, NY

Eubanks TM (1991) A consensus model for relativistic effects in geodetic VLBI. In: Eubanks TM (ed) Proceedings of the USNO workshop on relativistic models for use in space geodesy, pp 60–82

Eubanks TM, Matsakis DN, Martin JO, Archinal BA, McCarthy DD, Klioner SA, Shapiro S, Shapiro II (1997) Advances in solar system tests of gravity, American Physical Society, APS/AAPT Joint Meeting, 18–21 April, 1997 abstract #K11.05

Fomalont EB, Sramek RA (1975) A confirmation of Einstein's general theory of relativity by measuring the bending of microwave radiation in the gravitational field of the Sun. Astron J 199(3):749–755

Fomalont EB, Sramek RA (1976) Measurement of the solar gravitational deflection of radio waves in agreement with general relativity. Phys Rev Lett 36(25):1475–1478

Fomalont EB, Kopeikin SM (2003) The measurement of the light deflection from jupiter: experimental results. arXiv:astro-ph/0302294v2, pp 1–10

Heinkelmann R, Schuh H (2009) Very long baseline interferometry: accuracy limits and relativistic tests, In: Klioner SA, Seidelmann PK, Soffel MH (eds) Relativity in fundamental astronomy: dynamics, reference frames, and data analysis proceedings IAU symposium no. 261, Cambridge University Press

Hugentobler U (2008) Orbit Perturbations due to Relativistic Corrections. Unpublished notes available at ftp://maia.usno.navy.mil/conv2010/chapter10/add_info/

Huang C, Ries JC, Tapley BD, Watkins MM (1990) Relativistic effects for near-earth satellite orbit determination. Celest Mech Dyn Astron 48:167–185

Huang C, Liu L (1992) Analytical solutions to the four post-newtonian effects in a near-earth satellite orbit. Celest Mech Dyn Astron 53:293–307

Hoffman-Wellenhof B, Moritz H (2005) Physical geodesy. Springer-Verlag, Wien

Holdridge D (1967) An alternate expression for light time using general relativity, space programs, vol III. NASA, Washington, pp 2–4 (Summary 37–48)

Iorio L (2006) A critical analysis of a recent test of the lense–thirring effect with the LAGEOS satellites. J Geod 80:128–136

Iorio L (2007) The lense-thirring effect on orbits. In: Iorio L (ed) The measurement of gravitomagnetism. Nova Science Publishers Inc, NY, pp 73–86

Iorio L (2010a) On possible a priori "imprinting" of general relativity itself on the performed lense-thirring tests with LAGEOS satellites, communication and network, 2010, vol 2, pp 26–30. doi: 10.4236/cn.2010.21003 (Published Online February 2010 http://www.scirp.org/journal/cn)

Iorio L (2010b) Conservative evaluation of the uncertainty in the LAGEOS–LAGEOS II lense-thirring test. Cent Eur J Phys 8(1):25–32

Iorio L (2011) Effects of standard and modified gravity on interplanetary ranges. Int J Mod Phys D 20:181–232 (arXiv:1002.4585v5 [gr-qc])

Kaplan GH (2005) The IAU resolutions on astronomical reference systems time scales, and earth rotation models, explanation and implementation, United States Naval Observatory Circular No. 179, USNO, Washington

Kouba J (2004) Improved relativistic transformations in GPS. GPS Solutions 8:170–180

Klioner SA (1991) Proceedings of AGU chapman conference on geodetic VLBI: monitoring global change. In: Carter WE (ed) (NOAA Tech. Rep. NOS 137, NGS 49; Washington, DC: AGU), p 188

Klioner SA, Kopeikin SM (1992) Microarcsecond astrometry in space—relativistic effects and reduction of observations. Astron J 104:897–914

Klioner SA (2003) A practical relativistic model for microarcsecond astrometry in space. Astron J 125:1580–1597

Kopeikin SM (2001) Testing the relativistic effect of the propagation of gravity by very long baseline interferometry. Astrophys J 556:L1–L5

Kopeikin SM, Schäfer G (1999) Lorentz covariant theory of light propagation in gravitational fields of arbitrary-moving bodies. Phys Rev D 60:124002 (arXiv:gr-qc/9902030v5)

Lambert SB, Le Poncin-Lafitte C (2009) Determining the relativistic parameter γ using very long baseline interferometry. Astron Astrophys 499:331–335 (arXiv:0903.1615v1)

Larson KL, Ashby N, Hackman C, Bertiger W (2007) An assessment of relativistic effects for low earth orbiters: the GRACE satellites. Metrologia 44:484–490

Lebach DE, Corey BE, Shapiro II, Ratner MI, Webber JC, Rogers AEE, Davis JL, Herring TA (1995) Measurement of the solar gravitational deflection of radio waves using very-long-baseline interferometry. Phys Rev Lett 75(8):1439–1442

Lense J, Thirring H (1918) Uber die Einfluss der Eigenrotation der Zentralkorper auf die Bewegung der Planeten und Monde nach der Einsteinschen Gravitationstheorie. Phys Zeitschr, vol 19, p 156. English edition: Lense J, Thirring H (1984) Gen Relativ Gravitation (trans: Mashoon B, Hehl FW, Theiss DS (eds)), vol 16, p 711

Lindegren L (2009) Gaia: Astrometric performance and current status of the project, in: relativity in fundamental astronomy. In: Klioner SA, Seidelmann PK, Soffel MH Proceedings IAU symposium: dynamics, reference frames, and data analysis, proceedings IAU symposium no. 261, Cambridge University Press

Lucchesi DM (2003) LAGEOS II perigee shift and Schwarzschild gravitoelectric field. Phys Lett A 318:234–240

Lucchesi DM, Peron R (2010) Accurate measurement in the field of the earth of the general-relativistic precession of the LAGEOS II pericenter and new constraints on non-newtonian gravity. Phys Rev Lett 105:231103

MacMillan D, Petrachenko W, Niell A, Corey B, Behrend D, Schuh H (2011) VLBI2010: next generation VLBI System for geodesy and astrometry, Geophysical Research Abstracts, Vol. 13, EGU2011-13547, 2011, EGU General Assembly 2011

Margot J, Giorgini JD (2009) Probing general relativity with radar astrometry in the inner solar system. In: Klioner SA, Seidelmann PK, Soffel MH (eds) Relativity in fundamental astronomy: dynamics, reference frames, and data analysis, proceedings IAU symposium no. 261, Cambridge University Press

McCarthy DD, Petit G (2003) IERS conventions (2003), (IERS technical note; 32) Frankfurt am Maim: Verlag des Bundesamts für Kartographie und Geodäsie. Available at http://www.iers.org/nn_11216/IERS/EN/Publications/TechnicalNotes/tn32.html

Merkowitz SM (2010) Tests of gravity using lunar laser ranging. Living Rev Relativ, vol 13, p 7. Available at http://www.livingreviews.org/lrr-2010-7 (Online Article: cited on 12 Sep 2011)

Misner CW, Thorne KS, Wheeler JA (1973) Gravitation. W. H Freeman and Company, San Francisco

Moran J (1989) Introduction to VLBI. In: Felli M, Spencer RE (eds) Very long baseline interferometry, techniques and applications. Kluwer Academic Publishers, Dordrecht, pp 27–45

Moyer TD (2000) DESCANSO book series, deep space communications and navigation series. In: Yuen JH (ed) Formulation for observed and computed values of deep space network data types for navigation, vol 2

Montenbruck O, Gill E (2001) Satellite orbits: models, methods and applications. Springer-Verlag, Berlin

Müller J, Soffel M, Klioner SA (2008) Geodesy and relativity. J Geod 82:133–145

Murphy TW Jr, Adelberger EG, Battat JBR, Carey LN, Hoyle CD, LeBlanc P, Michelsen EL, Nordtvedt K, Orin AE, Strasburg CW, Stubss CW, Swanson HE, Williams E (2007) APOLLO: the apache point observatory lunar laser-ranging operation: instrument description and first detections. Publ Astron Soc Pac 120:20–37 2008 (arXiv:0710.0890v2)

Murphy T Jr (2009) Lunar ranging, gravitomagnetism, and APOLLO. Space Sci Rev 148:217–223

Newton I (1726) Principia: the mathematical principles of natural philosophy. English edition: (Motte A, Adee D), New York

Nelson RA, Ely TA (2006) Relativistic transformations for time synchronization and dissemination in the solar system. In: Proceedings of 38th annual precise time and time interval (PTTI) meeting. http://www.pttimeeting.org/archivemeetings/ptti2006.html, online article: cited on 9 May 2011

Neumann GA, Cavanaugh JF, Coyle DB, McGarry J, Smith DE, Sun X, Torrence M, Zagwodzki TW, Zuber MT (2006) Laser ranging at interplanetary distances. http://cddis.gsfc.nasa.gov/lw15/docs/papers/Laser Ranging at Interplanetary Distances.pdf, online article: cited on 11 Sept 2011. In: Proceedings of the 15th international workshop on laser ranging, Canberra, Australia

Pavlis DE, Poulose SG, Deng C, McCarthy JJ (2007) GEODYN II system documentation. SGT-Inc., Greenbelt, MD, contractor report

Perryman MAC, de Boer KS, Gilmore G, Høg E, Lattanzi MG, Lindegren L, Luri X, Mignard F, Pace O, de Zeeuw PT (2001) GAIA: composition, formation and evolution of the galaxy. Astron Astrophys 369:339–363

Petit G (2009) Relativity in the IERS conventions. In: Klioner SA, Seidelmann PK, and Soffel MH (eds) Relativity in fundamental astronomy: dynamics, reference frames, and data analysis. In: Proceedings IAU symposium no. 261, Cambridge University Press

Petit G, Luzum B (2010) IERS conventions (2010). In: Petit G, Luzum B (eds) (IERS Technical Note; No. 36). Bundesamts für Kartographie und Geodäsie, Frankfurt am Main. Available at http://www.iers.org/nn_11216/IERS/EN/Publications/TechnicalNotes/tn36.html

Pitjeva EV (2005) Relativistic effects and solar oblateness from radar observations of planets and spacecraft. Astron Lett 31:340–349

Robertson HP (1962) Relativity and cosmology. In: Deutsch AJ, Klemperer WB (eds) Space age astronomy. Academic, NY, pp 228–235

Robertson DS, Carter WE (1984) Relativistic deflection of radio signals in the solar gravitational field measured with VLBI. Nature 310:572–574

Robertson DS, Carter WE, Dillinger WH (1991) New measurement of the solar gravitational deflection of radio signals using VLBI. Nature 349:768–770

Ries JC, Huang C, Watkins MM (1988) Effect of general relativity on a near-earth satellite in the geocentric and barycentric reference frames. Phys Rev Lett 61:903–906

Riley WJ (2007) Handbook of frequency stability analysis. Hamilton Technical Services, USA, pp 22–23

Schuh H, Fellbaum M, Campbell J, Soffel M, Ruder H, Schneider M (1988) On the deflection of radio signals in the gravitational field of Jupiter. Phys Lett A 129:299–300

Schwarzschild K (1916) On the gravitational field of a mass point according to Einstein's theory. Sitzungsber Preuss AkadWiss, Phys Math Kl, vol 189, arXiv:physics/9905030v1, translated by S. Antoci and A. Loinger

Senior KL, Ray JR, Beard RL (2008) Characterization of periodic variations in the GPS satellite clocks. GPS Solut 12:211–225

Shapiro II (1964) Fourth test of general relativity. Phys Rev Lett 13:789–791

Shapiro II (1967) New method for the detection of light deflection by solar gravity. Science 157:806–808

Shapiro II, Pettengill GH, Ash ME, Stone ML, Smith WB, Ingalls RP, Brockelman RA (1968) Fourth test of general relativity: preliminary results. Phys Rev Lett 20:266

Shapiro SS, Davis JL, Lebach DE, Gregory JS (2004) Measurement of the solar gravitational deflection of radio waves using geodetic very-long-baseline interferometry data, 1979–1999. Phys Rev Lett 92(12):1–4 121101

Smith DE, Zuber MT, Xiaoli S, Neumann GA, Cavanaugh JF, McGarry JF, Zagwodzki TW (2006) Two-way laser link over interplanetary distance. Science 311:53

Soffel M, Klioner SA, Petit G, Wolf P, Kopeikin SM, Bretagnon P, Brumberg VA, Capitaine N, Damour T, Fukushima T, Guinot B, Huang T-Y, Lindegren L, Ma C, Nordtvedt K, Ries JC, Seidelmann PK, Vokrouhlicky′ D, Will CM, Xu C (2003) The IAU 2000 resolutions for astrometry, celestial mechanics, and metrology in the relativistic framework: explanatory supplement. Astron J 126:2687–2706

Sovers O, Fanselow J, Jacobs C (1998) Astrometry and geodesy with radio interferometry: experiments, models, results. Rev Mod Phys 70:1393–1454

Tapley BD, Schutz BE, Born GH (2004) Statistical orbit determination. Elsevier Academic Press, London

Turon C, O'Flaherty KS, Perryman MAC (eds) (2005) The three-dimensional universe with GAIA, ESA SP-576

Turyshev SG (2009) Experimental tests of general relativity: recent progress and future directions. Uspekhi Fizicheskikh Nauk, vol 179, p 3. arXiv:0809.3730 [gr-qc]

Turyshev SG, Farr W, Folkner WM, Girerd AR, Hemmti H, Murphy TW, Williams JG, Degnan JJ (2010) Advancing tests of relativistic gravity via laser ranging to Phobos. Experim Astron 28(2–3):209–249 (arXiv:1003.4961v2)

Vecchiato A, Lattanzi MG, Bucciarelli B, Crosta M, de Felice F, Gai M (2003) Testing general relativity by micro-arcsecond global astrometry. Astron Astrophys 399:337–342

Vallado DA (2001) Fundamentals of astrodynamics and applications, 2nd edn., Space technology libraryMicrocosm Press, California

Wei-qun Z, Chuan-fu L, Shuang-lin Y, Guan-zhong W, Yi-ping Z, Pei-hong Y, Jian Z (2001) A study and performance evaluation of hydrogen maser used in Chinese mobile VLBI stations. Chin Astron Astrophys 25(3):390–397

Will CM, Nordtvedt K Jr (1972) Conservation laws and preferred frames in relativistic gravity. I. Preferred-frame theories and an extended PPN formalism. Astrophys J 177:757–774

Will CM (2006) The confrontation between general relativity and experiment. Liv Rev Relativ. http://relativity.livingreviews.org/Articles/lrr-2006-3/, online article: cited on 12 Sep 2011, (arXiv:gr-qc/0510072v2)

Williams JG, Newhall XX, Dickey JO (1996) Relativity parameters determined from lunar laser ranging. Phys Rev D 53:6730–6739

Williams JG, Turyshev SG, Boggs DH (2004) Progress in lunar laser ranging tests of relativistic gravity. Phys Rev Lett 93:261101 (arXiv:gr-qc/0411113v2)

Williams JG, Turyshev SG, Boggs DH (2009) Lunar laser ranging tests of the equivalence principle with the earth and moon. Int J Mod Phys D 18:1129–1175 (arXiv:gr-qc/0507083v2)

Xu G (2007) GPS, theory, algorithms and applications, 2nd edn. Springer, Berlin

Zhang J, Zhang K, Grenfell R, Deakin R (2006) Short note: on the relativistic doppler effect for precise velocity determination using GPS. J Geod 80:104–110